# Stabilization of Pt Nanoparticles with Amine Ligands – An Alternative Approach to Supporting Nanoparticles for Catalytic Applications

## Dissertation

zur Erlangung des Doktorgrades der Naturwissenschaften

– Dr. rer. nat. –

des Fachbereichs 2 (Biologie/Chemie)

der Universität Bremen


vorgelegt von

*Eva Morsbach*

geboren in Bad Honnef

Bremen, 5. November 2014

Die vorliegende Arbeit wurde von Dezember 2011 bis November 2014 unter der Leitung von Herrn Prof. Dr. Marcus Bäumer am Institut für Angewandte und Physikalische Chemie der Universität Bremen durchgeführt.

**1. Gutachter** Prof. Dr. Marcus Bäumer
**2. Gutachter** Prof. Dr. Matthias Arenz
**Tag des Kolloquiums** 17.12.2014

# Selbstständigkeitserklärung

Hiermit erkläre ich, Eva Morsbach, dass ich die vorliegende Doktorarbeit mit dem Titel *Stabilization of Pt Nanoparticles with Amine Ligands – An Alternative Approach to Supporting Nanoparticles for Catalytic Applications* selbstständig verfasst und geschrieben habe und außer den angegebenen Quellen keine weiteren Hilfsmittel verwendet habe.
Ebenfalls erkläre ich hiermit, dass es sich bei den von mir abgegebenen Arbeiten um drei identische Exemplare handelt.

Bremen, 5.11.2014

# Mein Dank geht an...

**Prof. Marcus Bäumer** für die Möglichkeit, meine Promotion in deinem Arbeitskreis anzufertigen, für die Bereitstellung dieses innovativen und spannenden Themas und deine Unterstützung während der gesamten Promotion.

**Prof. Matthias Arenz** für die Bereitschaft als Zweitgutachter zur Verfügung zu stehen. Zusätzlich danke ich für die Gastfreundschaft in deiner Arbeitsgruppe und die große Unterstützung darüber hinaus.

**Dr. Sebastian Kunz** für die gute und inspirierende Zusammenarbeit, die vielen fruchtbaren Diskussionen und dafür, dass du nie die Geduld verloren hast.

**Eike Brauns** für die tolle und produktive Zusammenarbeit während des KatSense-Projekts. Ich habe mehr über Sensorik gelernt als ich erwartet hätte!

**Ute Melville, Cornelia Rybarsch-Steinke** und **Martin Nowak** für die großartige und vielfältige Unterstützung in jeglicher Hinsicht – ohne euch würde vieles einfach nicht laufen!

**Priv.-Doz. Dr. Volkmar Zielasek** und **Dr. Karsten Thiel** für die stetige Hilfsbereitschaft bei allen möglichen Fragen bzgl. des TEM.

**Eva-Maria Meyer** für den Spaß und das Interesse an meinen REM-Proben sowie den beeindruckenden Bildern, die daraus entstanden sind.

Der ganzen **AG Bäumer**, besonders **Ingo Bardenhagen, Andre Wichmann, Imke Schrader** und **Miriam Klink** für die nette Arbeitsatmosphäre über den rein fachlichen Austausch hinaus.

Der **AG Arenz**, besonders **József Spéder, Markus Nesselberger** und **Gustav Wiberg**, für die Gastfreundschaft und die Hilfe bei den elektrochemischen Messungen.

# List of Publications

Diese Dissertation wurde auf Basis folgender Veröffentlichungen angefertigt (in chronologischer Reihenfolge):

[I] E. Brauns, E. Morsbach, G. Schnurpfeil, M. Bäumer, W. Lang: "A miniaturized catalytic gas sensor for hydrogen detection based on stabilized nanoparticles as catalytic layer" *Sensors and Actuators B*, **2013**, *187*, 420–425.

[II] E. Brauns, E. Morsbach, S. Kunz, M. Bäumer, W. Lang: "A Fast and Sensitive Catalytic Gas Sensor for Hydrogen Detection based on Stabilized Nanoparticles as Catalytic Layer" *Sensors and Actuators B*, **2014**, *193*, 895–903.

[III] E. Morsbach, J. Spéder, M. Arenz, E. Brauns, W. Lang, S. Kunz, M. Bäumer: "Stabilizing Catalytically Active Nanoparticles by Ligand Linking: Toward Three-Dimensional Networks with High Catalytic Surface Area" *Langmuir*, **2014**, *30*, 5564–5573.

[IV] E. Morsbach, E. Brauns, T. Kowalik, W. Lang, S. Kunz, M. Bäumer: "Ligand-stabilized Pt nanoparticles (NPs) as novel materials for catalytic gas sensing: influence of the ligand on important catalytic properties" *PhysChemChemPhys*, **2014**, *16*, 21243–21251.

[V] E. Brauns, E. Morsbach, S. Kunz, M. Bäumer, W. Lang: "Temperature Modulation of a Catalytic Gas Sensor" *Sensors, Section Chemical Sensors*, **2014**, *14(11)*, 20372–20381.

[VI] E. Morsbach, Markus Nesselberger, Jonas Warneke, Matthias Arenz, Sebastian Kunz, Marcus Bäumer: "1-Naphthylamine functionalized Pt nanoparticles: Electrochemical activity and redox chemistry occurring on one surface", *submitted.*

Die aufgeführten Publikationen sind im Rahmen von Kooperationen und Zusammenarbeiten mit Kollegen aus verschiedenen Arbeitsgruppen und Instituten entstanden. Mein eigener Anteil an den genannten Publikationen wird im Folgenden erläutert.

- Für Publikation [I] und [II] wurden die funktionalisierten Nanopartikel (Katalysatoren) von mir entwickelt, hergestellt und charakterisiert sowie die entsprechenden Teile des Manuskriptes von mir verfasst. Desweiteren war ich an wissenschaftlichen Diskussionen bzgl. der Ergebnisinterpretation beteiligt.

- Für Publikation [III] lagen die Planung, Durchführung und Ergebnisinterpretation der Experimente sowie das Verfassen des Manuskripts in meiner Verantwortung. Die Sensor- und REM-Messungen wurden jedoch von Eike Brauns bzw. Eva-Maria Meyer (beide IMSAS, Universität Bremen) durchgeführt. Die Durchführung und Interpretation der elektrochemischen Messungen fand bei und mit Hilfe der AG Arenz statt. Ute Melville und Conny Rybarsch-Steinke übernahmen die Durchführung der AAS-Messungen.

- Für Publikation [IV] lagen Planung und Interpretation der Experimente sowie das Verfassen des Manuskripts in meiner Verantwortung. Die Herstellung der stabilisierten NP sowie die $H_2$-Oxidationsmessungen wurden von mir durchgeführt. Die Reflexion-IR Messungen wurden von Thomas Kowalik (IFAM Bremen) durchgeführt. Eike Brauns hat die Sensor-Messungen durchgeführt.

- Mein Anteil an Publikation [V] war die Katalysator-Herstellung und das Korrekturlesen des Manuskripts.

- Für Publikation [VI] lagen die Planung, Durchführung und Interpretation der Experimente sowie das Verfassen des Manuskripts in meiner Verantwortung. Die Herstellung der funktionalisierten NP-Katalysatoren führte ich durch. Die Durchführung und Interpretation der elektrochemischen Messung fand bei und mit Hilfe der AG Arenz statt. Ute Melville und Conny Rybarsch-Steinke übernahmen die AAS-Messungen.

# Deutsche Zusammenfassung

Nanopartikel (NP) zeigen, im Vergleich zu den analogen Festkörpern, einzigartige chemische und physikalische Eigenschaften. Aufgrund ihres großen Oberfläche-zu-Volumen-Verhältnisses und der daraus resultierenden hohen Oberflächenenergie neigen Nanopartikel jedoch zu Aggregation und Verschmelzung, wodurch die Nanostruktur verloren geht. Um die besonderen Eigenschaften von nanoskalierten Materialien zu nutzen, ist es daher essentiell, Nanopartikel zu stabilisieren und so die Nano-Struktur aufrecht zu erhalten.

Aus der Literatur sind verschiedene Ansätze zur Stabilisierung von Nanopartikeln bekannt. Beispielsweise ist es in der heterogenen Katalyse Stand der Technik, NP auf inerte anorganische Materialien (z. B. $Al_2O_3$) zu trägern, um Aggregation unter katalytischen Bedingungen zu verhindern. Allerdings ist es mittels dieses Ansatzes schwierig, das Verhältnis aktiver Oberflächenatome zur Katalysator-Gesamtmenge zu maximieren. Anwendungen wie z. B. thermoelektrische Gassensoren erfordern jedoch eine hohe Dichte an katalytisch aktiven Zentren bei einer gleichzeitig geringen Gesamtwärmekapazität, da dies das Antwortverhalten und die Höhe des Ausgangssignals bestimmt.

Ziel dieser Arbeit war es katalytische NP mit organischen Liganden zu stabilisieren, um eine Alternative zur klassischen Trägerung auf anorganischen Materialien zu entwickeln. Die katalytischen Eigenschaften derartig stabilisierter NP wurde im Rahmen dieser Arbeit examplarisch mittels eines thermoelektrischen Wasserstoff-Sensors untersucht. Um den Einfluss der Liganden auf die Materialeigenschaften zu identifizieren, wurden NP Synthese und Funktionalisierung in getrennten Schritten durchgeführt. Durch den Verzicht auf stark bindende Adsorbate während der Synthese können die NP effektiv mit verschiedenen Liganden funktionalisiert werden, so dass die Unterschiede der Materialien ausschließlich auf den Einfluss des Liganden zurückzuführen sind. Zur Stabilisierung wurden sowohl Mono- als auch Diamine verwendet.

Pt NP, die mit Monoaminen funktionalisiert wurden, sind nach der Synthese größtenteils mit Liganden bedeckt (Ligandenbedeckung 0,92–1). Die Untersuchung ihrer katalytischen Eigenschaften zeigte, dass die hohen Ligandenbedeckungen die katalytische Aktivität der Partikel nahezu vollständig unterdrücken. Die aktive Oberfläche lässt sich *in situ* durch partielle Ligan-

dendesorption vergrößern. Dadurch geht jedoch die stabilisierende Wirkung der Liganden verloren, so dass Aggregation der NP einsetzt und die aktive Oberfläche des Katalysators wiederum sinkt. Abschließend lässt sich sagen, dass Monoamine zur Stabilisierung von Pt NP mit dem Schwerpunkt katalytischer Anwendungen wenig geeignet sind. Zum einen ist die katalytisch aktive Oberfläche durch die hohe Ligandenbedeckung zu gering, und zum anderen ist die Stabilisierung der NP unter katalytischen Bedingungen unzureichend.

Daher wurde als Alternative zu den Monoaminen das Konzept der molekularen Verknüpfung von Nanopartikeln mit bifunktionellen Aminliganden eingeführt (*ligand-linking*). Es zeigte sich, dass Amin-verknüpfte Pt Nanopartikel dreidimensionale poröse Netzwerke mit ligandenfreien Oberflächenatomen bilden, die für katalytische Reaktionen zugänglich sind. Die ligandenfreien Oberflächenatome sind nach der Synthese mit CO bedeckt, welches in der Aktivierungsphase desorbiert. Somit werden die ligandenfreien Oberflächenatome zugänglich, und es lassen sich hohe katalytische Aktivitäten erreichen. Die Stabilität der ligandenverknüpften NP-Katalysatoren konnte im Vergleich zu den Monoamin-stabilisierten Nanopartikeln deutlich verbessert werden. Eine mögliche Erklärung dafür ist, dass während einer möglichen Desorption einer der beiden Kopfgruppen des bifunktionellen Liganden dieser durch die zweite Kopfgruppe im System verankert bleibt. Dies könnte eine anschließende Re-Adsorption der desorbierten Kopfgruppe ermöglichen, so dass die Stabilisierung der NP durch die Liganden aufrecht erhalten werden kann. Die stabilisierende Wirkung der Liganden ist jedoch nur gegeben, wenn diese intakt sind. Durch Untersuchung unterschiedlicher Ligandenstrukturen wurde festgestellt, dass ein Ligand zur erfolgreichen NP Stabilisierung in katalytischen Anwendungen ein aromatisches Kohlenwasserstoffgerüst anstelle eines Alkyl-Gerüstes haben sollte. Desweiteren ist das Vorhandensein von zwei möglichen Ankergruppen erforderlich, primäre Aminogruppen sind dabei tertiären Aminen aufgrund ihrer höheren Bindungsstärke zu Pt überlegen. Diese Kriterien werden von *para*-Phenylendiamin (PDA) erfüllt, wodurch der Ligand unter katalytischen Bedingungen stabil ist und durch das Verknüpfen von Pt NP mit PDA die Stabilisierung über mehr als 20 h kontinuierlichen Betriebs gewährleistet wurde. Somit konnte gezeigt werden, dass organische Liganden erfolgreich zur Stabilisierung katalytischer NP einsetzbar sind.

Die Anwendung des Monoamins 1-Naphthylamin (Napha) zeigt, dass Liganden nicht nur als „Zuschauer“ katalytische NP stabilisieren können, sondern auch selbst aktiv werden können: Napha-Pt NP, geträgert auf Kohlenstoff, zeigen eine elektrochemisch induzierte reversible Redoxreaktion des Liganden.

Nach einer Vorbehandlung lassen sich zusätzlich die Pt Oberflächenatome für elektrokatalytische Reaktionen (z. B. *CO stripping*) aktivieren. Somit wurde nicht nur ein System geschaffen, in dem der organische Ligand unter elektrokatalytischen Bedingungen stabil ist, sondern in dem zusätzlich eine parallel verlaufende elektrochemische Reaktion der Metall-Oberfläche und des Liganden nachgewiesen wurde.

# English Abstract

The state-of-the-art approach to stabilize nanoparticles (NPs) for heterogeneous phase applications is to support them on inert inorganic material, which is limited to low loadings of the catalytic compund. However, applications such as thermoelectric gas sensing require a high density of catalytically active sites at a low total heat capacity. To offer an alternative to the supporting of NPs, in this work the stabilization of catalytic NPs as solids with organic ligands was investigated. Mono- and bifunctional ligands were applied in this study. The catalytic properties of such stabilized NPs was exemplary investigated by application in a thermoelectric hydrogen sensor.

Pt NPs stabilized with mono-amines were almost completely covered with ligands, which almost completely suppresses the catalytic activity of the particles. In addition, the NPs aggregated over time, so that mono-amines do not facilitate sufficient stabilization of Pt NPs for catalytic applications.

The molecular linkage of Pt NPs with bifunctional amine ligands (*ligand-linking*) results in three-dimensional porous networks with ligand-free surface sites. In addition to an enhanced activity, the stability of the NPs can be significantly improved by ligand-linking. One reason may be that the bifunctional ligand is anchored on the NPs by two head groups. However, the NPs are only stabilized as long as the ligands are intact. The criteria for ligand structures to enable a successful NP stabilization were identified. *Para*-phenylenediamine (PDA) combines the criteria of aromatic hydrocarbon backbone and the presence of two $sp^3$ hybridized head groups. Consequently, by linking of Pt NPs with PDA a constant catalytic activity over more than 20 h on stream was achieved. Thus, organic ligands could be successfully applied to stabilize catalytic NPs.

Furthermore, the ability of ligands to participate in a reaction was shown: Pt NPs functionalized with the mono-amine 1-naphthylamine (NaphA) show a electrochemically induced reversible redox reaction of the ligand and simultaneous electrocatalytic reactions at the Pt surface. Thus, a hybrid material is formed which exhibits a parallel electrochemical reaction of the metal surface and the ligand.

# Contents

# List of Abbreviations

| | |
|---|---|
| AAS | **A**tomic **A**bsorption **S**pectroscopy |
| BiPy | 4,4'-**BiPy**ridine |
| CV | **C**yclic **V**oltammetry/**C**yclic **V**oltammogram |
| DAO | 1,8-**DiA**mino **O**ctane |
| EA | **E**lemental **A**nalysis |
| ECSA | **E**lectro**C**hemical accessible **S**urface **A**rea |
| EG | **E**thylene **G**lycol |
| HDA | n-**H**exa**D**ecyl**A**mine |
| HOMO | **H**ighest **O**ccupied **M**olecular **O**rbital |
| HSAB | **H**ard and **S**oft **A**cids and **B**ases |
| $H_{UPD}$ | **H**ydrogen **U**nder**P**otential **D**eposition |
| IMSAS | **I**nstitute for **M**icro**S**ensors, -**A**ctuators, and -**S**ystems, University of Bremen |
| IR | **I**nfra**R**ed |
| LUMO | **L**owest **U**noccupied **M**olecular **O**rbital |
| napha | 1-**Naph**thyl**A**mine |
| NMR | **N**uclear **M**agnetic **R**esonance |
| NP | **N**ano**P**article |
| PDA | *para*-**P**henylene**D**i**A**mine |
| RH | **R**elative **H**umidity |
| SAM | **S**elf-**A**ssembled **M**onolayer |
| SEM | **S**canning **E**lectron **M**icroscopy |
| TEM | **T**ransmission **E**lectron **M**icroscopy |
| VOC | **V**olatile **O**rganic **C**ompounds |

# 1 Motivation

Nano-sized materials are very fascinating due to their significantly different properties as compared to bulk materials. For catalytic applications, the advantage of nano-sized materials lies in their high surface-to-volume ratio, which enables to optimize the use of the catalytically active compound. [1] However, the unique chemical and physical properties of nano-materials are more interestingly, as it allows for the development of new materials. [2, 3]

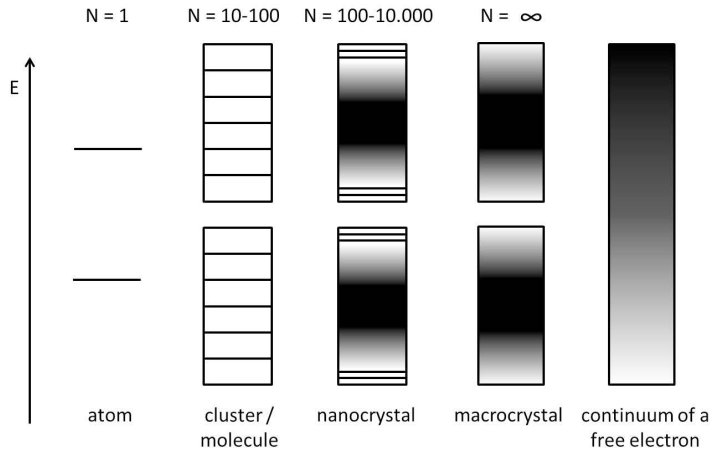


**Figure (1.1)** – *Simplified energy scheme for an atom, a molecule, a nanocrystal, a macrocrystal, and a free electron. For macroscopic particles, the energy levels overlap, forming quasi-continuous energy bands. In contrast, small systems have discrete energy levels with significant spacing between the discrete states. The electronic structure of nanocrystals is in-between, showing quasi-continuous energy bands with discrete energy levels at the band edges.*

Nanoparticles (NPs, in this work used synonymous for nanocrystals) usually consist of hundreds of atoms. Due to their sizes, the electronic properties of NPs are in-between that of single atoms and macroscopic crystals, as visualized in Fig. 1.1. [4, 5] In single atoms or molecules, the electrons are confined to discrete energy levels (s, p, d, ... or $\sigma, \pi, \delta$, ... orbitals, respectively). In macroscopic crystals, countless atomic orbitals overlap to numerous pseudo

"molecular orbitals" with insignificant differences in their energy, so that the electronic structure can be described by periodic combinations of atomic orbitals, and the energy levels can be considered as continuous. Hence, the energy levels are denoted as energy bands. The applied periodic boundary conditions neglect electronic effects of surfaces or crystal edges, which is reasonable for bulk material.

In nanoparticles, the number of overlapping orbitals is significantly lower as compared to macroscopic crystals, so that the effects of surface atoms on the electronic structure cannot be neglected. The energy level spacing depends on the particle size, so that the spacing of nanoparticles is larger as compared to bulk material but smaller as compared to molecules or clusters. The transition between discrete energy levels and a quasi-continuous band is smooth, and the particle size at which the states can be denoted as quasi-continuous depends on the specific elements. However, the concept of "bands" is often used to describe the electronic structure of NPs. [4] Due to the fact that the size of the particle influences the orbital overlap, even for nanoparticles of elements that form metallic macroscopic crystals a band gap is found for small particle sizes. [5–7] Although NPs of sufficient sizes show quasi-continuous energy levels, localized energy levels are present at the band edges, which result from the surface effects and influence the electronic structure of NPs. [3]

If the Fermi level of a nanoparticle is localized within the quasi-continuous region of an energy band (as known from metallic compounds), the electronic properties are similar to its bulk analog. In contrast, for semi conductor NPs the Fermi level is in general located at the discrete energy levels of a band edge, which consequently distinguishes its electronic properties from their macroscopic analog. [4] This effect is one of the major reasons for the broad interest on the electronic properties of semi-conductor nanocrystals, as the electronic structure of a material mainly determines its chemical properties.

In comparison to macroscopic crystals, NPs often show contractions of the crystal lattice and crystal defects. Due to the high curvature of small spherical NPs, the number of neighbored atoms on the surface is low, and the orbital overlap between neighbored surface atoms is reduced. As a result, the surface atoms are both coordinatively and electrically unsaturated, which explains their high reactivity. [3] Another consequence of the reduced number of neighboring atoms is a high mobility of the surface atoms. NPs thus exhibit higher vapor pressures and a lower melting point than their corresponding bulk materials. [5, 8] In addition, nano-materials show a large amount of grain boundaries and a high surface energy, which results in their strong tendency toward sintering and coalescence. [9] The stabilization of NPs in order to

maintain the nanosized particles hence is prerequisite for any application. [3]

In heterogeneous liquid-phase and gas-phase catalysis, the state-of-the-art method to stabilize NPs is to support them on inert inorganic material. The loading with the active compound, however, is limited to small values (single-digit weight percentages), which limits the density of catalytically active surface sites. In applications like catalytic gas sensing based on a thermoelectric working principle, a high density of active sites at a low total catalyst mass is desired in order to achieve a fast response and a high sensitivity. [10, 11] Consequently, the deposition of catalytic NPs on support material suppresses a good performance, and alternative strategies toward NP stabilization are desired.

So far, the stabilization of NPs by ligands or capping agents (organic molecules bound to the NP surface) has been mainly reported in colloid chemistry in order to stabilize NPs during synthesis and subsequently in a dispersion. [12] In the following, I will distinguish between the terms "capping agent" and "ligands" to differentiate between applying adsorbates during NP synthesis to prevent coalescence (capping agent) and a target-oriented functionalization of NPs for specific applications (ligands). Within my PhD project, I investigated the potential of organic ligands for the stabilization of catalytic NPs as solids. This appraoch represents an alternative to the stabilization by supporting NPs and is expected to enable a high density of active sites. The NPs were functionalized with different ligands, and their catalytic potential was exemplarily investigated with a thermoelectric gas sensor.

In order to exclusively relate differences of the material properties to the influence of the ligand, a preparation protocol is required that allows for a separation of NP synthesis and functionalization. Due to the fact that capping agents do not only stabilize the NP colloid but influence the synthesis and the resulting NPs in terms of size and size dispersity, morphology, and anisotropic growth of specific crystal facets ("faceting"), [13–15] a synthesis route was chosen with minimal influence of capping agents during the synthesis. In this way, the ligand of interest can easily and effectively be functionalized to the NPs via ligand exchange subsequent to the synthesis, and the differences in the material properties can be related exclusively to the influence of the ligand. My work concentrated on the stabilization of Pt NPs with amine ligands, since Pt exhibits a high catalytic activity for a number of reactions, and amines are known to effectively bind to Pt. [16] Two different types of amines were applied in this study, namely mono- and bifunctional amines. Chapter 2 describes the wet-chemistry synthesis of NPs and the stabilization

of colloids, while Chapter 3 describes the strategies towards NP stabilization as solids. The functionalization with mono-amines and bifunctional amines is described in Chapter 4 and 7, respectively. The stabilizing effect of mono- and diamines on Pt NPs was investigated by their application as catalysts in thermoelectric hydrogen sensors (the sensor and its working principle is introduced in Chapter 5), which is described in the Chapters 6 and 8–9, respectively. Finally, I investigated the potential to utilize the chemical properties of a ligand instead of merely using it as a stabilizer. The redox activity of a ligand was found during the application of functionalized NPs in electrochemistry and is described in Chapter 10.

# 2 Synthesis and stabilization of NP colloids

In this chapter, the general concept of wet-chemistry NP synthesis as well as different synthetic approaches are introduced. In addition, the requirements of NPs for this study are discussed, followed by the characterization of the NPs obtained by the applied polyol process.

NPs can either be prepared by bottom-up (utilizing atomic precursors) or top-down approaches (macroscopic crystals serve as starting material). For scientific interests, the advantages of bottom-up approaches outweigh their disadvantages, such as small batch sizes and difficulties in up-scaling of production processes. [17] Bottom-up wet-chemistry syntheses most often allow for an individual and effective adjustment of synthetic parameters. Consequently, a precise control over particle size, size distribution, morphology, and composition as well as a high reproducibility can be achieved. [18] Colloidal syntheses are an example of a wet-chemistry bottom-up approach where the resulting NPs are stabilized in a solvent and any aggregation or sedimentation is suppressed. [12] Colloids are defined to be substances in a fine dispersed state with particle sizes below 100 nm, so that dispersions of NPs in a solvent can be denoted as colloids. [3]

## 2.1 Formation of monodisperse NP colloids

Wet-chemistry syntheses of metallic nanoparticles (NPs) are very versatile as they are accessible for nearly all monometallic as well as bimetallic systems. [18–27] The formation of metal colloids by chemical reduction of transition metal salts in the presence of stabilizing agents was first introduced by Faraday in 1857. [28]

A well-established model to describe the formation of monodisperse particles has been introduced by LaMer and has been adopted for colloidal NPs. [18, 29] The generation of crystals is initiated by the formation of nucleation seeds, that subsequently grow into bigger crystals. The essential key for generating

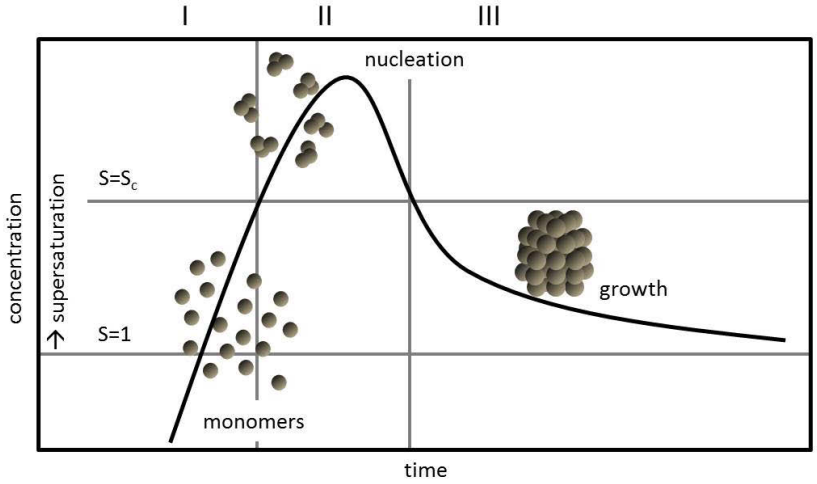


**Figure (2.1)** – *LaMer plot: Change of supersaturation as a function of time. The degree of supersaturation determines the different stages during colloid formation, namely nucleation and growth. Modelled in the style of [18].*

monodisperse NPs is to establish an identical growth history for the individual particles, which can be achieved by separation of nucleation and growth. Hence, the seed formation (nucleation) has to be limited to a short period of time, after which only growth takes place without further nucleation. This concept is referred to as *burst of nucleation*.

Fig. 2.1 visualizes the different stages of nanocrystal formation from metal precursors according to the *burst of nucleation* concept. Prior to nucleation, crystal monomers (the mininum subunit of the bulk crystal) have to be released from the metal precursor (stage I). For Pt NPs, the minimum subunit is a Pt atom. Two main approaches can be distinguished for the formation of the subunites: A metal salt can be applied as precursor where the metal cation is reduced to the atomic monomer by a reducing agent upon *heating-up* the reaction mixture. Alternatively, a zero-valent metal-organic precursor which is unstable at elevated temperatures can be used. Upon injection into the hot reaction mixture, the precursor is decomposed to release the metal atom (*hot-injection*). [18, 30]

In both approaches, the monomer concentration constantly increases over time during stage I. Due to the high energy barrier for homogeneous nucleations, even under supersaturated conditions ($S > 1$) no nucleation takes place until the critical supersaturation $S_C$ is exceeded (stage II). Now the energy barrier for homogeneous nucleation can be overcome, so that stable crystallization

nuclei are formed. The monomer concentration decreases during the nucleation, because the rate of monomer consumption exceeds the rate of monomer supply. Consequently, seed formation continues until the monomer concentration drops below the critical supersaturation, after which the net nucleation rate is zero (stage III). Further released monomers add to already formed seeds, and the particles will grow as long as the solution is supersaturated.

Under the assumption of a sufficiently short time period for nucleation (stage II), all NPs will have a similar growth history and the resulting NP will have a correspondingly narrow size distribution (monodispersity). Because synthesis parameters (choice of reactants and solvents, reaction temperatures, heating ramps *etc.*) strongly influence both the nucleation and the growth, they will consequently determine the quality of the resulting NPs. Therefore, the synthesis of NP colloids is very versatile. However, the synthesis parameters have to be chosen carefully and be optimized with regard to the desired NP size and dispersity. [31, 32]

## 2.2 Stabilization of NP colloids

Due to the high surface energy of NPs, the colloids have to be stabilized in order to prevent agglomeration and further growth of the individual particles. In general, stabilizing agents need to be applied already during synthesis. The different strategies toward stabilization of colloidal NPs, which all employ the help of stabilizing reactants, can be categorized into three main concepts, namely electrostatic repulsion, inhibited diffusion (*e.g.* synthesis in micelles), and steric hindrance (by binding capping agents or coordinating polymers to the NP surface). The different concepts are sketched in Fig. 2.2.

The electrostatic stabilization is based on Coulomb repulsion between NPs that is mediated by an electric double layer of ions surrounding the NPs, see Fig. 2.2 a). For example in Au sols prepared by the Turkevich method, the colloidal particles are surrounded by citrate and chloride ions as well as cation counterions. [4, 33] When the distance between two particles is reduced, the diffuse parts of their double layers will overlap. If the electric potential of the double layers is sufficiently strong, a repulsive electric potential will prevent further approaching. As a result, agglomeration of the NPs is prevented and the NPs are stabilized. [34] The effectiveness of the electrostatic stabilization depends on the ionic strength of the dispersing medium. A low electrolyte concentration increases the range of the double layer repulsion and, hence, enhances the colloid stability. If the ion concentration is increased (*e.g.* by

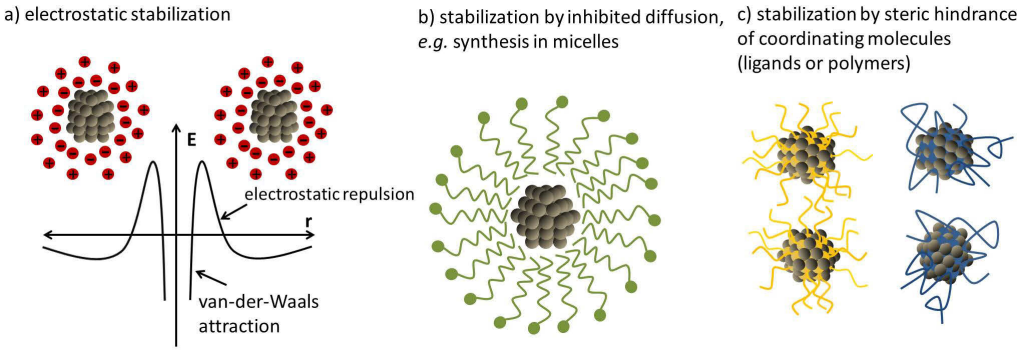


**Figure (2.2)** – *Sketch of the different strategies toward the stabilization of NP colloids: a) electrostatic repulsion*[1]*, b) inhibited diffusion by synthesis in a micelle, and c) steric hindrance by binding of coordinating molecules,* e.g. *ligands or polymers, to the NP surface.*

the addition of a salt), the electrical repulsion is shielded and aggregation of the particles is induced by the resulting van-der-Waals attraction. [34] The electrostatic stabilization of NPs is difficult to adjust and maintain, as slight changes in the ionic strength of the system may lead to a loss of the stabilization effect and cause aggregation.

The concept of NP synthesis in (reverse) micelles was established by Pileni *et al.* The idea is that the inner core of a micelle constitutes a "nanoreactor", in which the formation of ideally one NP per micelle occurs, as sketched in Fig. 2.2 b). Thereby, the agglomeration of the formed NPs is inhibited by the surrounding micelle. The size and shape of the NPs are a result of the conditions inside the micelle, which can be influenced by the choice of the surfactants. [35–37] However, the formation of monodisperse spherical Pt NPs by applying the micelle approach has been found to be challenging, because control over the micelles and their stabilizing properties can be complicated. [38] The crystallinity of NPs synthesized in micelles is often poor as a consequence of the restriction to low reaction temperatures ($T < 100$ °C) in micelle reactions. [18]

Steric stabilization denotes the binding of molecules to the NPs that prevent approaching of two NPs, as sketched in Fig. 2.2 c). Most often, long-chained or branched hydrocarbons, or even coordinating polymers, are applied to establish an organic shell around the NPs. [30, 39] These molecules are coordinatively or even covalently bound to the surface via an anchoring or head group (a

[1] Designed in the style of [30]

functional group that is able to bind to the NP), such as amines, thiols, or phosphines. [30] Two forces influence the success of steric stabilization, namely the interaction between head group and surface atom as well as the intermolecular ligand-solvent interaction. [12, 40] The bond between NP and head group is determined by the electronic properties of metal and functional group, so that the Pearson concept of hard and soft acids and bases can be used as a rule of thumb to estimate the binding strengths. [41, 42] Assuming that the size of the ligand tail is sufficiently large to attentuate a possible surface charge of the NP, the stability of the dispersion is determined by the interaction between ligand and solvent. Thus, the intermolecular forces between ligand molecules or between ligand and solvent (*e.g.* van-der-Waals interaction) should be considered. [43] If two NPs stabilized with long-chain alkyl ligands approach each other in a dispersion, the alkyl chains may interdigitate, induced by attractive van-der-Waals forces. [44, 45] However, the interdigitation cannot be extended over the entire length of the molecules due to geometric restrictions. Consequently, the NPs are kept apart from each other, and coalescence is prevented. Additionally, the interdigitation of the alkyl chains will lower the entropy of the system, while the attractive interaction between ligand and solvent will support a state of dispersed NPs. Hence, agglomeration of the sterically stabilized NPs in an dispersing solvent is prevented by the steric barrier of the ligands that keep the NPs at a distance.

In this work I will refer to *capping agents* as stabilizers applied during NP synthesis, while the term *ligand* will be used for molecules that are bound the to NPs subsequent to their synthesis. The application of capping agents during NP synthesis to prevent aggregation, precipitation, or to obtain shape control is widely applied. A commonly used capping agent for Pt NPs is oleylamine (often in combination with oleic acid), due to the effective coordination of amines to Pt. [46, 47] The reduction of the metal precursor has a strong influence on the nucleation and formation of NPs. The reactive metal precursor can be equivalent to the applied metal reactant or can be formed *in situ* via coordination of solvent molecules or capping agents toward the metal core. [12] In this way, the application of a capping agent directs the rates of precursor reduction and as a result influences nucleation and NP formation. [12, 46] Consequently, the size, shape, crystallinity, and faceting of NPs can be adjusted by the choice of the capping agent. However, a ligand exchange subsequent to the synthesis may be difficult if the capping agents bind strongly to the NPs.

The addition of coordinating polymers (commonly used is *e.g.* PVP) or block-copolymers in NP synthesis has as well been broadly established for the syntheses of metal NPs, as the long chains and the high amount of functional

groups provide effective steric stabilization. [32,48–51] Therefore, polymers can either coordinate to the metal precursor prior to its reduction or to the formed NPs via their functional groups. [19] One advantage of polymer-assisted NP synthesis is the possibility to precisely control the resulting particle sizes by adjusting the ratio between polymers and metal precursor. [52] Due to the length and the large number of functional groups in a polymer chain, the accessibility of the surface is suppressed and the polymer has to be removed before catalytic applications. [53, 54] Polymer-assisted syntheses for catalytic NPs are hence disadvantageous considering that polymer removal requires harsh conditions. [30]

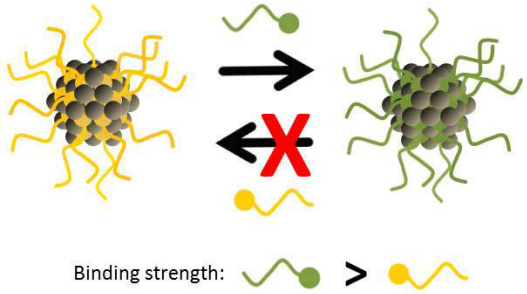


**Figure (2.3)** – *Sketch of ligand exchange of two monofunctional ligands. The direction of the exchange is determined by the binding strength toward the NP.*

The preparation of NP colloids with the help of steric stabilization allows for versatile and tailored NP syntheses. In order to investigate the influence of the ligand on the material properties, NP synthesis and functionalization with the ligand of interest, which will be performed via ligand exchange, should be separated into individual steps. As sketched in Fig. 2.3, the success of the ligand exchange is determined by the different binding strengths toward the NPs. [55–57] Strongly binding adsorbates applied during synthesis may hinder effective and complete functionalization subsequent to the synthesis. In order to enable an effective ligand exchange, a synthetic protocol is desired with minimum influence of capping agents, which allows for effective ligand exchange subsequent to NP synthesis.

## 2.3 Polyol synthesis of Pt nanoparticles

The so-called polyol synthesis is a synthesis strategy for colloidal NPs that has its origin in the formation of $MeO_x$ particles synthesized by reducing metal

salts in ethylene glycol. However, these particles precipitate after synthesis due to their micrometer dimensions. [58, 59] The appraoch has been extended to the synthesis of noble metal particle colloids that are found to be successfully stabilized in alkaline polyol. [60]

The main advantage of the polyol approach is that no additional capping agents are needed, as the polyol can fulfill three requirements: The polyol serves as solvent, reducing agent, and enables the colloid stabilization. In this way, only the metal precursor and the (alkaline) polyol is present in the reaction mixture. The polyol may stabilize small noble metal NPs, but is however no strongly binding adsorbate. The most frequently used polyol is ethylene glycol (EG, ethane-1,2-diol), as it allows for reaction temperatures up to 200 °C and has the highest reduction potential as compared to oligo-ethylene glycols. [31]

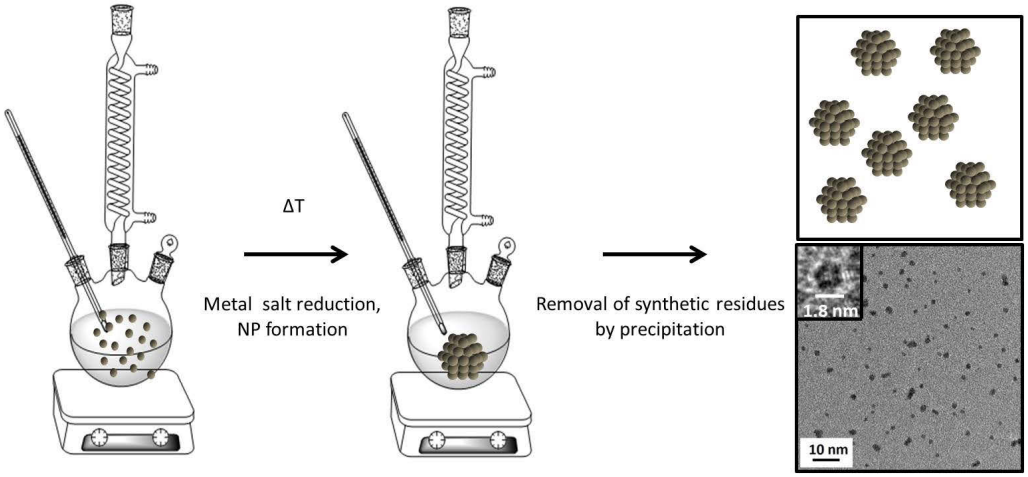


**Figure (2.4)** – *Polyol synthesis of platinum nanoparticles. Upon heating, the metal precursor $H_2PtCl_6$ is reduced by alkaline ethylene glycol to form "unprotected" Pt NPs (the NPs are referred to as "unprotected" as no strongly binding adsorbates are added during synthesis). After synthesis, the NPs are washed and the synthesis residues are removed.*

In this work, a preparation route for platinum NPs known from literature was applied for all particle syntheses. [61] A sketch of the synthesis strategy and a representative TEM image of the resulting Pt NPs are shown in Fig. 2.4. Upon heating, the metal salt $H_2PtCl_6$ is reduced by alkaline ethylene glycol to form the crystallization monomers (Pt atoms), which subsequently nucleate and grow to form Pt NPs. The resulting NP size of 1.8 nm corresponds to a dispersion (ratio of surface atoms to total number of atoms per NP) of

0.56. The synthesis is highly reproducible and insensitive to disruptions of *e.g.* heating ramp or reaction temperature.

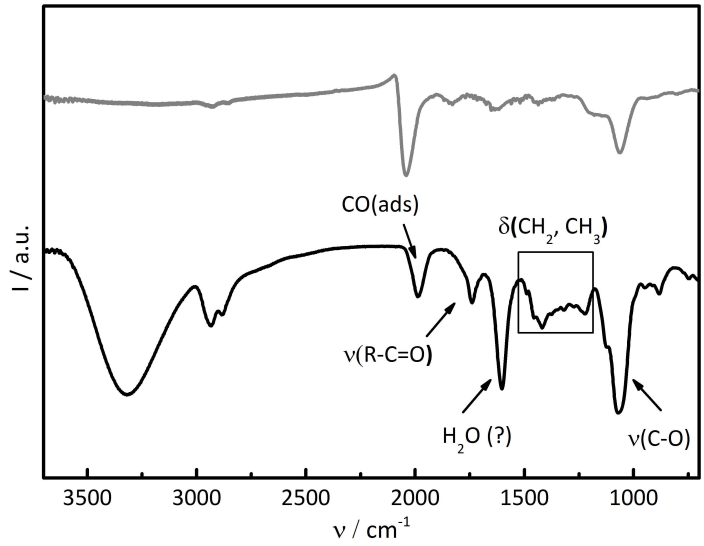


**Figure (2.5)** – *IR-Spectra of "unprotected" Pt NPs. Black: Isolation of Pt NPs by changing polarity of the solvent. Grey: Pt NPs precipitated with HCl and subsequent washing.*

In this work, the as-prepared NPs are referred to as "unprotected" due to the fact that no strongly binding capping agent or ligand is present. However, a stable NP colloid requires an attractive interaction between solvent and NPs that is considered to be mediated by adsorbents on the NP surface. The precise mechanism of NP stabilization in the polyol approach is not clear yet and difficult to elucidate. Possible adsorbates stabilizing the NP surface that are present in the reaction mixture are ethylene glycol or its oxidation products (glycolic and oxalic acid), carbon monoxide (side product of EG decomposition), and chloride ions. [62] IR spectra of "unprotected" Pt NPs isolated from the reaction mixture by precipitation with unpolar solvents (Fig. 2.5, black graph) reveal the large amount of molecules adsorbed on the NP surface. Parts of the organic residues can be removed by precipitating and washing the NPs with HCl and water (Fig. 2.5, grey graph). The remaining synthesis residues are no strongly binding adsorbates and, consequently, allow for subsequent functionalization. After the washing procedure, redispersion of the NPs in polar solvents is possible as the solvents overcome the interparticle attraction by attractive interaction with the adsorbates on the NP surface. [13]

In summary, the major advantage of the polyol approach is the absence of strongly binding adsorbates during NP synthesis that allows for subsequent manipulation of the surface. Residual adsorbates from synthesis can be exchanged by strongly binding ligands, *e.g.* amines, thiols, or phosphines, which is demonstrated in the following chapters. As a result, the "unprotected" NP colloids can serve as basic building blocks for the selective functionalization with specific ligands subsequent to the synthesis.

# 3 Strategies for NP stabilization as solids

Due to the high surface energy of NPs, stabilizing agents are required not only during synthesis, but especially for heterogeneous gas-phase or liquid-phase applications. [9] In this chapter, the state-of-the-art strategy for NP stabilization by supporting is introduced. Subsequently, the idea of NP stabilization with ligands, especially organic amines, is discussed.

## 3.1 Deposition of NPs on inert support material

For applications in heterogeneous gas-phase or liquid-phase catalysis, NPs are mainly stabilized by supporting them on inert inorganic materials, as sketched in Fig. 3.1. [63, 64] Metal oxides like $Al_2O_3$ or $SiO_2$ are commonly used for gas-phase or liquid-phase catalysis, while high surface area carbons are state-of-the-art supports in electrocatalysis. [65, 66]

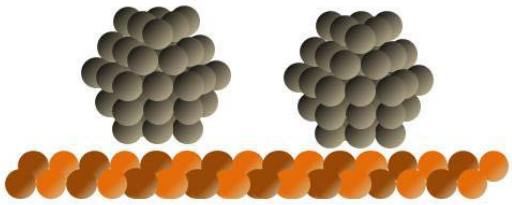

**Figure (3.1)** – *Deposition of NPs on inert support material. The application of so-called* supported NPs *is the state of the art approach for NP stabilization in heterogeneous phase applications.*

At elevated temperatures the deposited NPs may become mobile on the support. [9] In order to prevent the NPs from agglomerating, which would result in a loss of the active surface area, the metal loadings in heterogeneous catalysis have to be kept low ($< 10$ wt%). Consequently, low ratios of catalytically active sites to the total amount of applied material result. [67] For applications that require high densities of active sites, the use of inorganic

support materials thus has limited applicability. An alternative approach for the stabilization of catalytic NPs was hence investigated in this work and is introduced in the following section.

## 3.2 Ligand-stabilized NPs as solids

As already introduced above, the attractive interaction between ligand and solvent prevents agglomeration of NPs in a dispersion. However, upon deposition of ligand-functionalized NPs onto a substrate and subsequent solvent evaporation, the ligand-ligand interactions between adjacent NPs become predominate. Alkyl chains as the simplest representative of hydrophobic ligands experience intermolecular van-der-Waals attraction, such that the deposited NPs locate themselves in close vicinity. It has been found that the distance between two adjacent alkyl stabilized NPs is less than twice the lengths of the linearly extended (*all-trans*) alkyl chains, which is explained by an interdigitation of the ligand tails. [44, 45, 68] An increase of the alkyl chain length leads to an increase of the attractive intermolecular interactions (around 4 kJ/mol per $CH_2$ unit) and, hence, supports a close arrangement. [8] Monodisperse NPs with long-chained hydrophobic ligands can even self-assemble into ordered superlattices with the closest packing of an hcp or fcc structure. [45, 69] The conformational flexibility of the alkyl chains enables space filling of the voids between the NP spheres. [68]

However, the ligand interdigitation cannot proceed over the whole length of the alkyl chain for steric reasons. Consequently, the steric hindrance of the ligand tail still keeps the NPs at a distance and, thereby, supports NP stabilization even as solids.

A second concept of sterical NP stabilization with ligands can be achieved with bifunctional ligands. The conceptional idea of the so-called *ligand-linking* is to bind one ligand to two NPs to ensure a certain spacing between the NPs and, thereby, prevent agglomeration. Ligand-linking of NPs has already been applied in a non-catalytic context. For example, thin films of dithiol-linked Au NPs have been prepared by layer-by-layer deposition and applied in resistive gas sensing by Joseph *et al.* [70, 71] The intermolecular interaction of volatile organic compounds (VOCs) with the linking ligands was found to change the electric resistance of the film and enables the detection of such molecules. [71, 72] However, no catalytically active ligand-linked NPs have been reported so far.

As the distances between ligand-functionalized NPs are determined by the

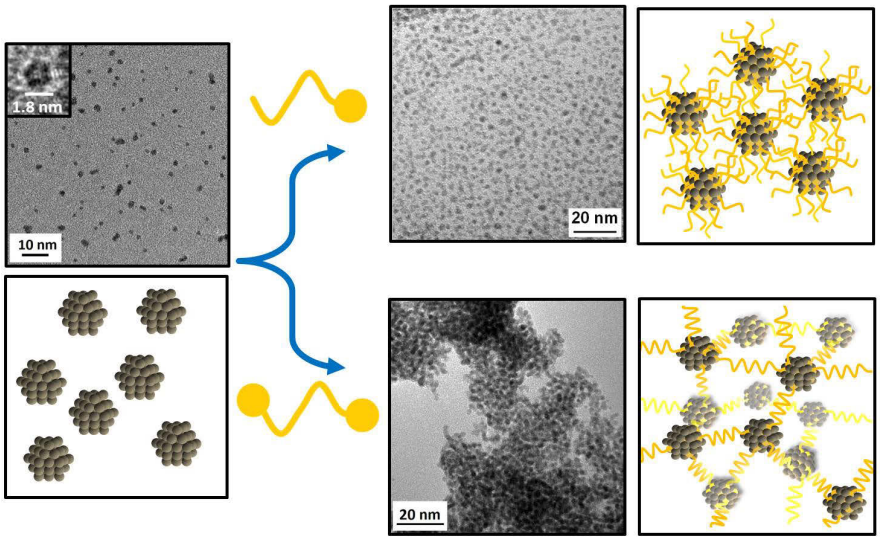


**Figure (3.2)** – *Starting from "unprotected" NPs that result from the polyol process, the NPs can be functionalized with different mono- or bifunctional ligands. In this way, the material properties like its stability in catalytic applications can be related exclusively to the influence of the ligand.*

molecular sizes of the ligands, the stabilization of catalytic NPs with organic ligands promises a high density of active sites in the catalytic material. Fig. 3.2 sketches the applied preparation route toward ligand-stabilization. The synthesis of "unprotected" NPs via the polyol process allows for functionalization of the NPs with different mono- or bifunctional ligands in a separate step. In this way, different properties of ligand-functionalized NPs, *e.g.* their stability in catalytic applications, can be related exclusively to the influence of the ligand.

# 4 Stabilization of Pt NPs with mono-amines

## 4.1 Functionalization with mono-amines

Amines were chosen for the stabilization due to their good binding properties toward Pt. [41, 73] Regarding the HSAB concept, amines as well as Pt are classified as "soft", which allows for an effective binding. The amine group forms a dative bond to the Pt surface via the lone pair of electrons, while the ligand tail provides a steric stabilization and directs the dispersibility of the functionalized NPs in solvents. According to the binding strength of amines on Pt, they are assumed to be in a dynamic adsorption-desorption equilibrium, which is distinctively shifted to the adsorbed state under ambient conditions.

Stabilization with ligands could also be achieved by functionalizing the NPs with thiols, which are known to form strong (covalent) bonds with noble metals. [74] Thiols were however found to be not suitable for catalytic applications, as they fully inhibit the catalytic activity of the Pt NPs.

Pt NPs can be functionalized with mono-amines via replacement of weaker binding adsorbates, which is denoted as *ligand exchange* (*vide supra*, Fig. 2.3). To readily indicate the success of ligand binding, functionalizations are often executed as phase transfer reactions. Fig. 4.1 visualizes the functionalization of "unprotected" NPs with an alkylamine which is accompanied by a phase transfer of the NPs. Therefore, the NPs are dispersed in a polar medium (*e.g.* ethylene glycol, utilizing the as-prepared NP colloid, here: blue), while the ligand (alkylamine) is dissolved in a nonpolar solvent (*e.g.* toluene, here: red) that is not miscible with the polar medium. Upon mixing of both phases, the ligands bind to the NPs (denoted as functionalization). As a consequence of the nonpolar ligand tail, the functionalized NPs are transferred to the nonpolar phase which exhibits attractive interaction with the ligand shell. A color change of both phases indicates the successful phase transfer.

In colloid chemistry, phase transfer reactions are often employed as a one-pot reaction during NP syntheses, if the necessary capping agent is of inverse

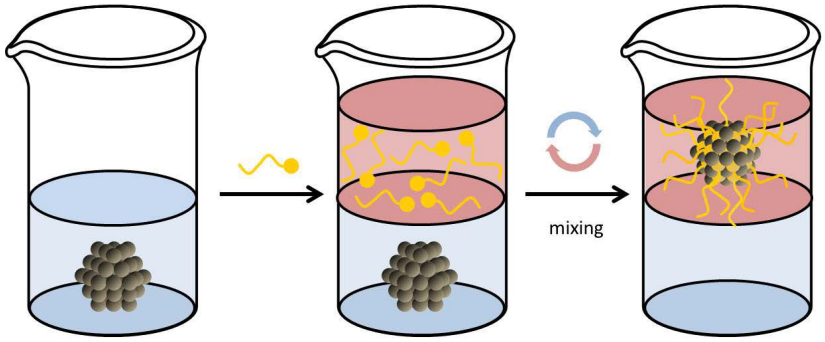


**Figure (4.1)** – *Functionalization of a Pt NP with mono-amines, accompanied by phase transfer of the functionalized NP.*

polarity to the metal precursor. For example, many metal precursors are only soluble in aqueous media, while the required reducing or capping agents are hydrophobic. [38, 75, 76] In these cases, a biphasic reaction is performed which requires an additional phase transfer agent. (Compare, for example, the Brust-Schiffrin method. [77])

The drawback of a biphasic reaction, however, is the poor compatibility of most reactants. The capping agent has to be compatible with all other reactants, including the reducing agents (such as $NaBH_4$) and phase transfer agent. Surface impurities on the resulting NPs that are often caused by the phase transfer agent have to be excluded. [77] In addition, the formation of very small NPs has been found to be difficult in biphasic NP syntheses. [77] Thus, the separation of NP synthesis and functionalization into subsequent steps to circumvent a biphasic reaction is advantageous.

Phase-transfer reactions by ligand exchange can also be applied as a tool to adjust the NP dispersibility and, consequently, enable specific NP applications. For example, bio-medical applications (cell targeting, contrast agents for MRI, ...) require dispersibility and colloidal stability in aqueous media, while the NP syntheses are often only accessible in organic media. [78, 79] Thus, subsequent functionalization with hydrophilic ligands, which is accompanied with a phase transfer, provides the desired hydrophilicity of the NP shell. [80,81]

In contrast, heterogeneous liquid-phase catalysis is often performed in nonpolar solvents. In order to ensure a stable NP deposition on the support material, a hydrophilic ligand shell is employed, which implements a repulsive interaction between NP catalyst and solvent. [82, 83]

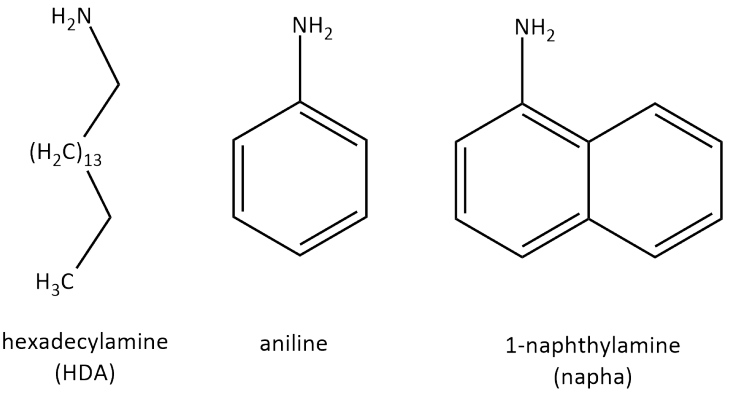


**Figure (4.2)** – *Structural formula of the monofunctional ligands used in this work.*

The structural formula of the monofunctional ligands discussed in this thesis, namely hexadecylamine (HDA), aniline, and 1-naphthylamine (napha), can be found in Fig. 4.2. Due to their nonpolar hydrocarbon backbones, all functionalizations can be performed as phase transfer reactions from the as-prepared Pt NP dispersion in ethylene glycol (Pt-EG) to organic solvents (see Fig. 4.1). The resulting mono-amine stabilized Pt NPs are characterized in terms of morphology of deposited assemblies, changes in the ligand structure upon functionalization and application, and presence of catalytically active surface sites.

## 4.2 Characterization of mono-amine stabilized Pt NPs

The assembly of hexadecylamine stabilized Pt (HDA-Pt) NPs upon deposition is presented in Fig. 4.3. A monolayer of the deposited NPs (TEM image, b)) is found to assemble in close vicinity to each other without exhibiting a long-range order. The long alkyl chains may interdigitate, as sketched in Fig. 4.3 a), which may cause the dense arrangement of the HDA-Pt monolayer. The flat and dense arrangement is maintained for multilayers (Fig. 4.3, c)), as demonstrated by the SEM image. The bright spots correspond to individual NPs.[1] For comparison with the loosely spread assembly of unprotected NPs, see Fig. 2.4.

Deposited monolayers of aniline-Pt NPs look similar to HDA-Pt. However,

[1]The Gemini Auriga40 SEM with InLens detector allows for a resolution down to 1 nm which enables to visualize individual NPs that are displayed as bright spots.

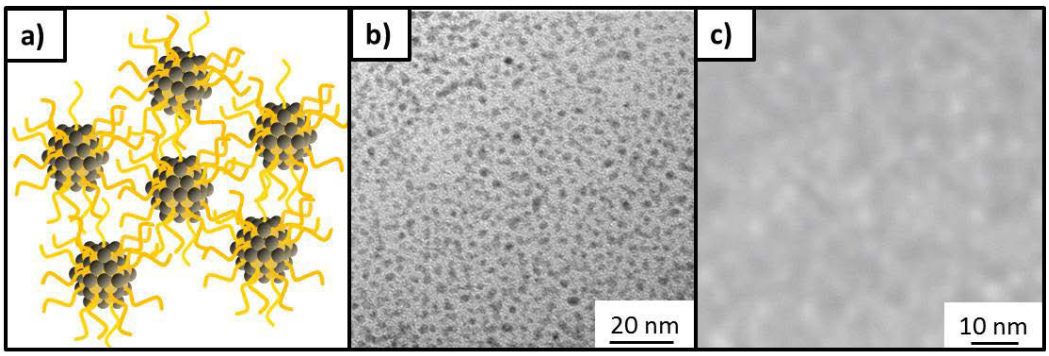


**Figure (4.3)** – *Arrangement of HDA-Pt NPs upon deposition and solvent evaporation. Left: Sketch to visualize the interdigitation of the alkyl chains. Middle: TEM image of a monolayer of HDA-Pt NPs. Right: SEM image of a multilayer deposition of HDA-Pt NPs.*[1]

one has to keep in mind that the intermolecular interactions differ between alkyl- and aryl-moieties. For example, ligand tail interdigitation cannot take place at phenyl moieties. The different intermolecular interactions become obvious in the multi-layer assembly. The resulting branched flake-like morphology of deposited multi-layers of aniline-Pt NPs is shown in Fig. 4.4. In contrast to alkyl systems, aromatic systems can assemble in a stacked order induced by $\pi$-$\pi$ interaction, [84, 85] which may be the reason for the different multilayer assembly of aniline-Pt.

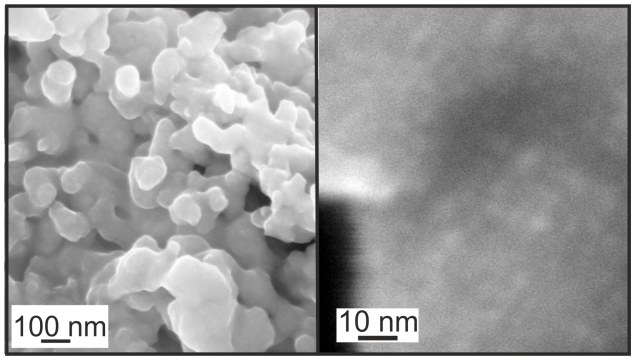


**Figure (4.4)** – *SEM images of deposited aniline-Pt NPs. Multilayers of aniline-Pt NPs assemble into a branched structure (left). A zoom into the branches (right) demonstrates that the branches consist of individual NPs.*[1]

[1]The Gemini Auriga40 SEM with InLens detector allows for a resolution down to 1 nm which enables to visualize individual NPs that are displayed as bright spots.

The ligand shell can be investigated by *e.g.* IR and NMR spectroscopy. As already introduced above, the dative bond of an amine ligand results in a shift of electron density from N (p-orbital) to the d-orbitals of Pt [42] and can be compared to the coordination chemistry in metal-organic complexes. [86] Due to the fact that ligands bound to NPs experience a changed chemical environment, the NMR signals are shifted compared to the pure ligand. Furthermore, the proton signals of alkyl ligands broaden upon functionalization, which is strongly pronounced for protons in the vicinity of the NP surface. [41] The shift and broadening of the signals are attributed to the changed electron density of the ligand upon binding as well as to electromagnetic shielding of the metal particle.

For alkyl isocyanides bound to Pt NPs it has been reported that the N≡C vibration changes upon functionalization, which is caused by a shift of electron density from the ligand to Pt. [86] Due to the fact that binding of amines to Pt results in a shift of electron density from N to Pt as well, the vibrations of the ligand may also experience changes.

The changed ligand vibrations that can be followed by IR spectroscopy are representatively shown for aniline-Pt in Fig. 4.5. The spectrum of "unprotected" Pt NPs has already been discussed above in Chapter 2. In the spectrum of aniline-Pt (Fig. 4.5 left), the characteristic vibrations of aniline like C=C, $NH_2$, or C-H vibrations are present which indicates successful functionalization with intact ligand molecules. In Fig. 4.5 (right), the aniline vibrations are shown in more detail. The characteristic vibration pattern of the aromatic C=C ring stretching (around 1600/1515/1450 $cm^{-1}$) is maintained upon functionalization, while the individual vibrations are shifted by several wave numbers. The corresponding vibrations are marked in the spectra by arrows. Additionally, the $NH_2$ scissoring mode around 1625 $cm^{-1}$ vanishes, while a new vibration caused by the N-Pt interaction arises at 1580 $cm^{-1}$. In reports about the coordination of aniline or alkyl amines to transition metals, the phenomenon has been assigned to a shift of the $NH_2$ scissoring mode. [87, 88] A red shift of the vibration is believed to be caused by the shift of electron density from N to Pt [42], which would also result in a changed hybridization of N, and by an anchoring of the otherwise conformationally unrestricted amine group. [87, 88] Due to the fact that a vibration at around 1580 $cm^{-1}$ was found in our group even for non-primary amines, the vibration cannot be assigned to a $NH_2$ scissoring mode, but is identicaled as characteristic for amines on Pt NPs. [89] The changed chemical environment of the ligand can additionally be visualized by the arise of vibrations between 3000–2800 $cm^{-1}$. However, until now we could not elucidate to which vibration these

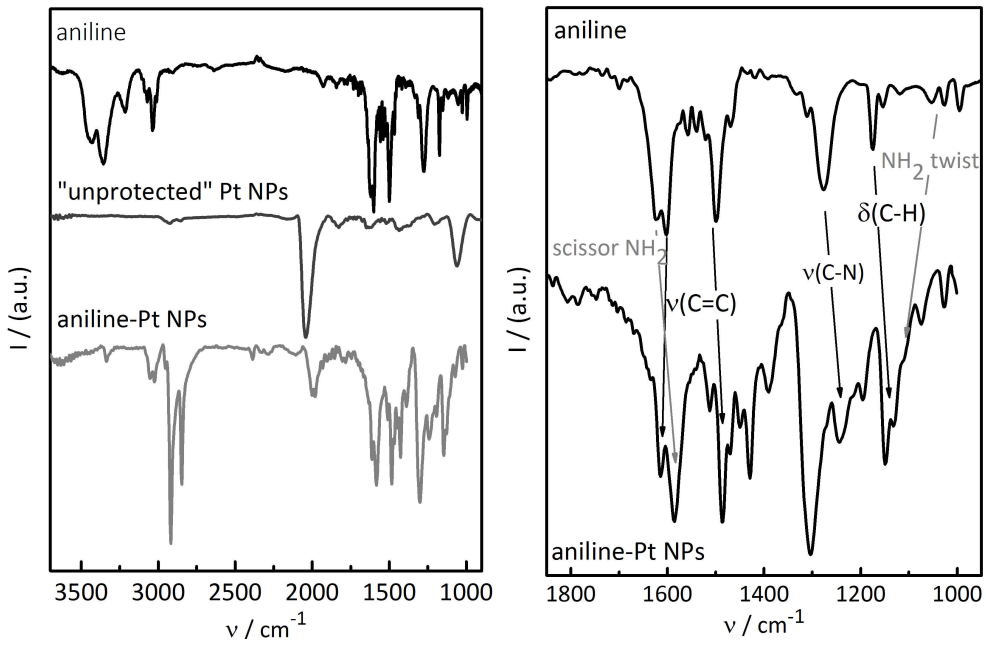


**Figure (4.5)** – *IR spectra of ligand functionalization. Left: aniline-Pt NPs compared to the pure ligand and "unprotected" NPs. Right: effect of functionalization on the aniline vibrations. The vibration assignment is based on [87].*

bands can be assigned. It may be possible that the force constants of the aromatic C-H stretching, which are usually found at $\nu > 3000$ cm$^{-1}$, may change upon functionalization, such that vibrations between 3000–2800 cm$^{-1}$ result. (The IR spectra of HDA-Pt and napha-Pt NPs are shown and discussed in Publikation [III] and [V], respectively.)

In a NP dispersion, the amine ligands on Pt are assumed to be in a dynamic adsorption-desorption equilibrium with the heat of adsorption determining the state of adsorption. [40] At ambient conditions, the equilibrium is shifted to the adsorbed state. Nonetheless, the amine ligands can re-arrange or can be removed from the surface, *e.g.* by washing or aging. [90, 91] The resulting ligand coverage can be investigated by a combination of atomic absorption spectroscopy (AAS), elemental analysis (EA), and transmission electron microscopy (TEM, for size determination). The correlation of AAS and EA allows for quantification of the elemental ratios between Pt and C, H, and N. With the measured NP sizes (TEM), the number of surface atoms can be calculated, which enables the determination of the number of ligand molecules per surface atom, which is denoted as ligand coverage. However,

since HDA-Pt NPs cannot be isolated well enough to achieve a solvent-free powder sample without excess of unbound ligands and solvent, AAS/EA measurements did not deliver reliable results for the ligand coverage.

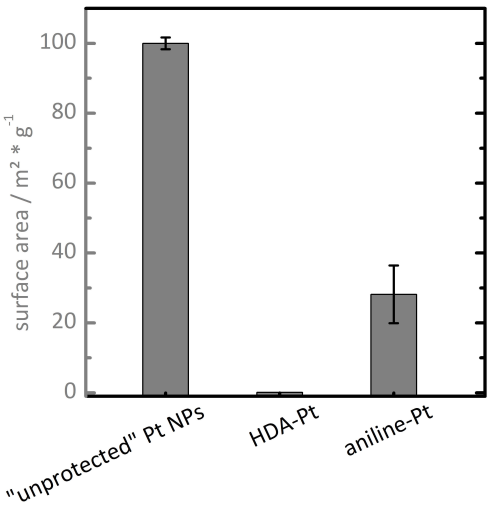


**Figure (4.6)** – *ECSA of "unprotected" and mono-amine functionalized Pt NPs, determined by hydrogen under potential deposition ($H_{UPD}$). Therefore, the NPs were deposited on glassy carbon electrodes without further fixation or support.*

An alternative approach to determine the ligand coverage of catalytic metal surfaces is the quantification of the catalytically active surface sites which are expected to be uncovered by ligands. Cyclic voltammetry (CV) can be applied as a tool for the elucidation of the electrochemically accessible surface area (ECSA). In the course of the potential cycles in an acidic electrolyte, hydrogen (or, more precisely, protons) is electrochemically adsorbed (and desorbed) on ligand-free Pt surface sites. [92, 93] On Pt, the deposition of H takes place at potentials negative compared to the double layer region until hydrogen ($H_2$) evolution, and is denoted as hydrogen underpotential deposition, $H_{UPD}$. [94] Protons originating from the electrolyte are adsorbed under consumption of one electron with an stoichiometry of one H atom per Pt surface atom, according to:

$$H^+ + Pt + e^- \rightleftharpoons H - Pt \tag{4.1}$$

Consequently, the transferred charge corresponds to the amount of adsorbed hydrogen and, hence, accounts as a measure for the number of ligand-free Pt surface sites. With the knowledge about the electrode loading and the particle

size, the ligand coverage (number of ligand molecules per surface atom) can be determined from the ECSA of functionalized Pt NPs. ECSA of "unprotected", aniline- and HDA-stabilized Pt NPs are presented in Fig. 4.6. Ligands with little steric demands like *n*-alkyl amines can form a full monolayer on NPs (1 ligand per surface atom). [95] The absence of any significant peaks in the CV of HDA-Pt NPs indicates that the surface atoms are completely covered and, consequently, not accessible for (electro-)catalytic reactants. A free surface area of only 0.1 $m^2/g$ Pt was determined. For comparison, the "unprotected" Pt NPs showed an ECSA of around 100 $m^2/g$. As a result, a full ligand coverage on HDA-Pt NPs was confirmed by cyclic voltammetry.

The introduction of a ligand backbone with steric demands was found to result in the creation of ligand-free surface sites: Due to its aromatic hydrocarbon skeleton, aniline has higher steric demands and, consequently, an ECSA of 28 $m^2/g$ results for aniline-Pt NPs (see Fig. 4.6). This value is still low as compared to "unprotected" Pt NPs, but it demonstrates how catalytically accessible surface sites can be created through the choice of the ligand.

# 5 Catalytic hydrogen sensing with Pt NPs

Reports about catalytic gas sensors with NP catalysts merely concern NPs stabilized on an inorganic support, adopting strategies from gas phase catalysis. [96–98] However, the catalyst loading on the support is usually limited to low amounts, which limits the ratio of catalytic surface sites to the overall catalyst mass and, consequently, the overall sensor performance. Therefore, ligand-stabilized Pt NPs were tested on their performance in catalytic gas sensing, as the stabilization with ligands enables to achieve a high density of active sites in the material.

In this chapter, the sensor principle of thermoelectric hydrogen sensors and its requirements for high performance catalysts are introduced. The sensor used in this study is characterized in order to determine suitable experimental parameters.

## 5.1 Introduction into catalytic hydrogen sensing

Catalytic gas sensing denotes the detection (and quantification) of gases by catalytic conversion (combustion), which triggers the sensor signal. In general, gas sensing with Pt NPs as catalyst is possible for all volatile molecules that can be catalytically converted by Pt via an exothermic (or theoretically also endothermic) reaction. The main focus of this work lied on hydrogen sensing due to its high industrial relevance. [10]

Fig. 5.1 illustrates the thermoelectric hydrogen sensor developed by the IMSAS[1] and its working principle. The sensor design and working principle are described in detail in Publications [I] and [II]. The functionalized Pt NPs are deposited onto the catalyst membrane, which is connected to a heater and thermopiles. The heater ensures the stable operating temperature. Thermopiles are electronic devices in which an electric potential arises upon a temperature difference between both ends (junctions) of the thermopiles

[1] Institute for microsensors, -actuators and systems, University of Bremen, project partner

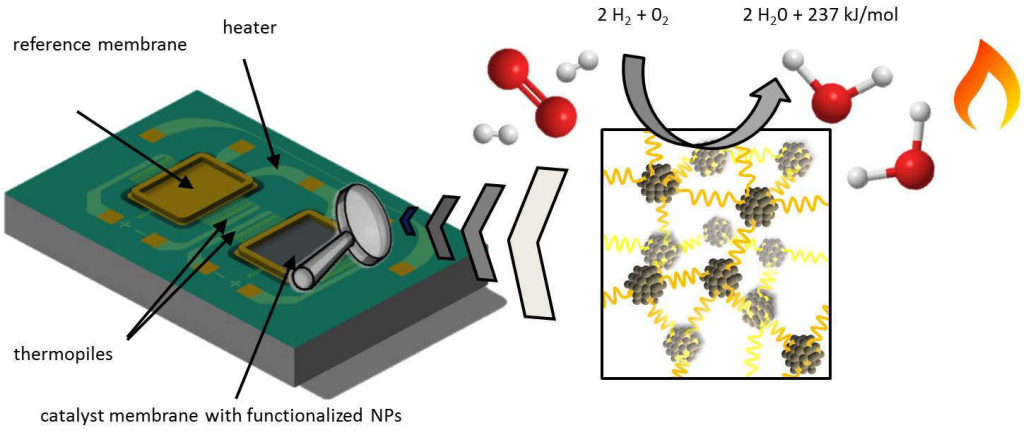


**Figure (5.1)** – *Catalytic gas sensor with functionalized NPs as catalyst. The reactant gases diffuse to the catalyst, where they are catalytically converted. As a result, the exothermic heat of reaction induces the sensor signal.*

(Seebeck effect). The gas molecules, in this work hydrogen in synthetic air, diffuse into the catalyst. On the NP surface, the reactants ($H_2 + O_2$) are converted to water. The exothermic heat of reaction induces a temperature difference at the thermopiles, which causes the sensor signal (electric potential) with the Seebeck coefficient being the constant of proportionality. As a result, there is a linear relationship between hydrogen conversion and height of the sensor signal.

Due to the sensor's operating principle, a good sensor performance requires a low heat capacity of the catalyst with a good thermal isolation of the catalyst membrane, a high ratio of catalytic surface sites to catalyst mass, and a small catalyst volume to enable high sensitivity and short response times. Of course, a good long-term stability of the catalyst is desired as well. The high weight ratio between Pt ($\sim$ 70 wt%) and ligands ($\sim$ 30 wt%) as well as the high surface-to-volume ratio of the NPs (diameter $\sim$ 1.8 nm) makes the material promising for their application on catalytic gas sensors.

## 5.2 Determination of the sensor's properties

The investigation about the sensor's properties were conducted with the ligand-linked NP catalyst PDA-Pt, which exhibits sufficient long-term stability and activity. Further description of the material and its sensor performance can be found in Chapter 7 and 8.

The correlation between hydrogen partial pressure and sensor output has been investigated by stepwise increasing and subsequently decreasing the hydrogen partial pressure and recording the output signal. The sensor response toward 1000 ppm and 20 ppm steps is presented in Fig. 5.2. As expected for catalytic gas sensors, ligand-linked NP catalysts show a linear dependency between the partial pressure of hydrogen and sensor output. A clear resolution can be achieved down to 20 ppm $H_2$, while at around 10 ppm of $H_2$ the electrical noise becomes dominant.

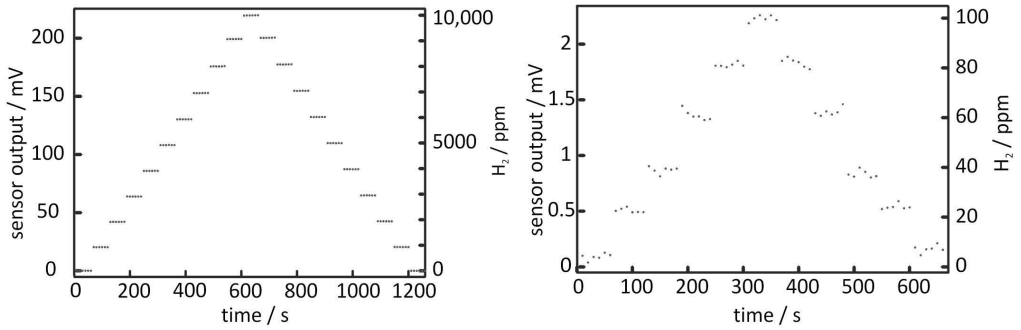


**Figure (5.2)** – *Dependence of the sensor output on the hydrogen partial pressure. The hydrogen concentration was stepwise increased and subsequently decreased with step sizes of 1000 ppm (left) and 20 ppm (right). The operating temperature and humidity was kept constant. The linear correlation between hydrogen partial pressure and sensor output is one of the main advantages of catalytic gas sensors over other sensor principles.*

The response time of a sensor is an important characteristic. In thermoelectric sensors the response time does not only depend on the electronics and the diffusion of the reactants to the catalyst. Additionally, the heat capacity and thermal conductivity of the catalyst has a strong influence on the response time, as the sensor output is induced by a temperature change of the catalyst. The high density of active sites enables a fast catalytic conversion of the reactant gas, resulting in a very short response time of the sensor (90 % response within $< 150$ ms). No significant differences of the response time was found for different ligands. In contrast, the response time of commercially available hydrogen sensors lies around 8 s, [10] and thermoelectric hydrogen sensors with $Al_2O_3$ supported Pt catalysts have response times of $\geq 7$ s. [96,97] Further details about the response time can be found in Publikation [II].

The operating temperature significantly influences the height and the stability of the sensor signal. At low operating temperatures (*e.g.* 70 °C) the output

of the sensor shows a steep decline. In general, a reason for a decreased reactant conversion at lower temperatures, which would in turn lead to a lower sensor output, may be simply a decreased reaction rate according to the Arrhenius equation. The investigations of Hanson and Boudart concerning the $H_2$ oxidation on supported Pt demonstrated this correlation between temperature and reaction rate. [67] However, a slow reaction rate may cause a low sensor output, but should enable a constant signal. Due to the fact that no stable output was observed at 70 °C operating temperature, but the sensor output declines to zero, another explanation may be more suitable. The declining sensor output could be caused by hampered desorption and diffusion of $H_2O$ formed within the reaction. Even the deposition of condensed water within the small pores is conceivable. As a consequence, the surface sites may be blocked for further reactant conversions. A decrease of the hydrogen oxidation rate caused by product water vapor has already been reported by Hanson *et al.* for supported Pt catalysts. [67] The deposition of water may be detectable by *operando* spectroscopic measurements that were, however, not possible to be integrated into this work, but will be part of a future project.

If the operating temperature is too high (110 °C) the sensor output decreases as well, but with a slight decline. At higher temperatures undesired side reactions like ligand desorption and subsequent decomposition become more favorable, thus leading to destruction of the catalyst, as the stabilization effect is lost.

The optimum operating temperature was determined to be 90 °C, as this temperature allows for a constant sensor operation.

# 6 Catalytic properties of mono-amine stabilized Pt NPs in hydrogen sensing

Pt NPs stabilized with mono-amine ligands (HDA and aniline) were applied as catalysts in hydrogen sensing. The sensor measurements were performed with a constant stream of 1 vol% hydrogen in synthetic air, and the sensor output was recorded over time. The results are displayed in Fig. 6.1. The sensor signal has been converted from the electric potential to the generated temperature difference $\Delta$T to account for different Seebeck coefficients of individual sensors. Activation behavior, sensitivity (height of sensor signal for a given hydrogen partial pressure), and long-term stability of HDA-Pt and aniline-Pt are discussed and compared to "unprotected" Pt NPs. For a more detailed discussion on the results, see Publication [IV].

"Unprotected" Pt NPs as catalysts produce a high sensor signal after a very short activation phase, see Fig. 6.1 (left), while the stability is very poor and the sensor output drops rapidly. Due to the absence of strongly adsorbed molecules, see Chapter 2, the surface atoms are accessible for the reactants without preceding cleaning processes, which results in the short activation phase. At the same time, due to the absence of strong adsorbates as stabilizers, the NPs sinter quickly, which reduces the catalytic surface area. [9] As a consequence, the reactant conversion is diminished, which leads to the deteriorated sensor signal.

In contrast, the sensor signal of HDA-Pt catalysts is negligible under standard operating conditions. Due to the full ligand coverage, the surface atoms are not accessible for the reactants. The activity can be increased at higher operating temperatures (150 °C) and with a long activation phase (about 5 h). At high temperatures, the ligands may partially desorb and, thereby, create catalytically accessible surface sites. However, the activity increase of HDA-Pt NPs caused by partial ligand desorption takes place at expense of the stabilization. The desorption of ligands initially increases the amount of ligand-free surface sites, leading to enhanced reactant conversion. But

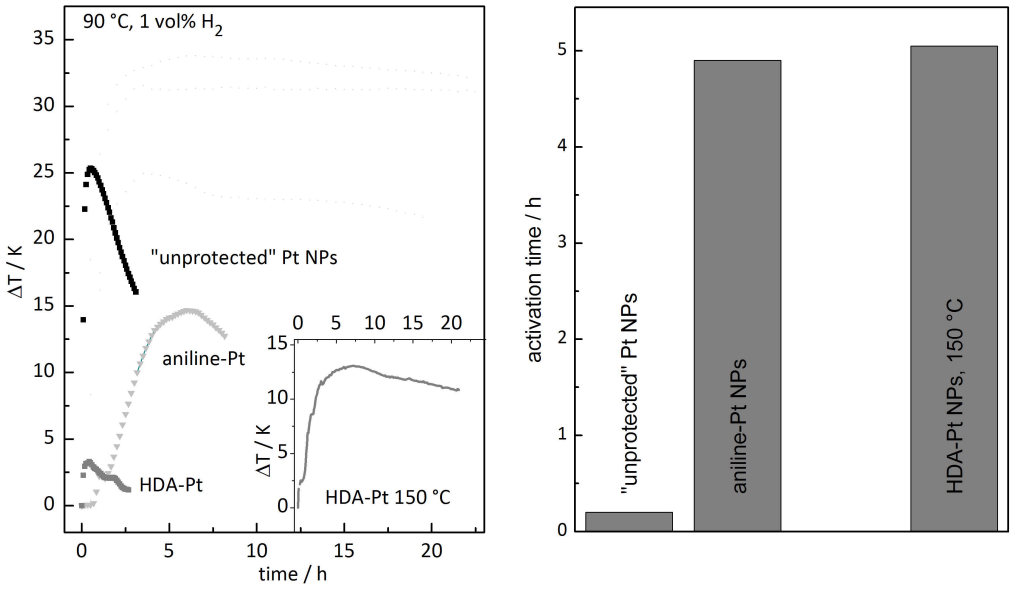


**Figure (6.1)** – *Sensor performance with mono-amine functionalized Pt NPs, in comparison to "unprotected" Pt NPs, for hydrogen detection. Left: Sensor output converted to the generated temperature difference during a long-term measurement under a constant stream of gas. Right: Time period to achieve maximum sensor output, denoted as activation time, derived from the long-term measurement.*

the investigation of the ligand structure before and after hydrogen sensing by IR spectroscopy revealed that HDA molecules are subject to oxidation and decomposition of, among others, the amine head group during sensing. The IR spectra before and after $H_2$ oxidation and discussion of the ligand structure are shown in Fig. 6.2, further details on the activation behavior and ligand decomposition can be found in Publication [IV]. Destroyed ligand molecules cannot stabilize the NPs. As a result, the active surface area of the NP catalyst decreases, which diminishes the reactant conversion, and the sensor looses its sensitivity.

In contrast to HDA-Pt, aniline-Pt catalysts showed a significant sensor signal at standard operating temperature. However, the activation period was around 5 h. As discussed above, the steric demand of the aromatic backbone introduces ligand-free surface sites on the functionalized NPs that enable catalytic reactions. After preparation, the ligand-free surface sites are covered with CO, which has to be removed in order to allow for catalytic reactions. The binding strength of CO to Pt is weaker than the binding strength of amines,

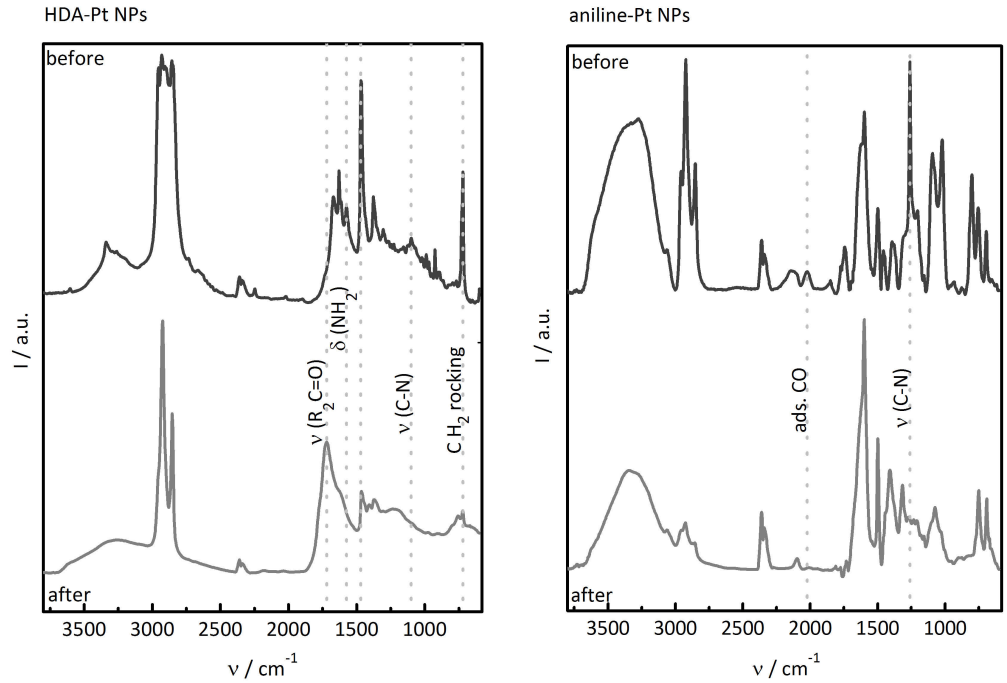


**Figure (6.2)** – *Reflection-mode IR spectra of mono-amine stabilized Pt NPs before and after $H_2$ oxidation. For HDA-Pt, the $NH_2$ deformation vibration and the C-N vibration are vanished after gas sensing experiments, indicating that the amine group is cleaved from the alkyl chain. Additionally, the $CH_2$ rocking vibration, which only occurs when at least three methylene units are connected in a linear mode, as well as the C-H deformation vibration have almost disappeared. In contrast, a distinct vibration of a carbonyl group (aldehydes or ketones) arose, indicating that the alkyl group is cleaved or oxidized. For aniline-Pt NPs, the adsorbed CO is removed after the sensor measurements, indicating that during the activation phase the CO desorbs and catalytically active surface sites are created. During the sensor experiments the aromatic system is maintained. The C-N vibration, however, is vanished, indicating a cleavage and destruction of the amine head group, such that the stabilization effect is lost.*

which enables the selective desorption of CO in order to create uncovered Pt surface sites. [99, 100] IR spectra of aniline-Pt NPs before and after hydrogen conversion confirm the desorption of CO, as shown in Fig. 6.2. After several hours of hydrogen oxidation, the cleavage of the C-N bond of aniline and decomposition of the amine group was detected. Similar to the destruction of HDA molecules, the decomposition of aniline during the sensor operation

diminishes the stabilization effect on the NPs, which gives way to NP sintering and results in a decreased catalytically active surface area. Thereby, the sensor output deteriorates over time.

The results of the sensor measurements with HDA-Pt and aniline-Pt catalysts and the associated IR studies revealed that Pt NPs functionalized with mono-maines are not sufficiently stabilized for catalytic applications. In addition, the sensor output is low, even with the presence of ligand-free surface sites. In order to create stable and active catalysts for gas sensing, another concept for NP stabilization is required.

# 7 Ligand-linked NPs

## 7.1 Concept of ligand linking

As introduced above, the idea of ligand-linking is to bind one ligand between two NPs in order to keep them at a distance and prevent agglomeration. Three-dimensional networks can be build from NPs and bifunctional ligands. A material results with its properties depending on the ensemble (which denotes the collectivity of individual particles) of NPs and the ligands.

In literature, studies can be found about ligand-linked NP thin films and investigations about their optical and electrical properties. For example, an ensemble effect of the NPs in close proximity can be visualized by the optical properties of a Langmuir-Blodgett film or even multilayer assemblies of alkyl dithiol linked Au NPs. [6,8] Shipway and Wang have reported that the surface plasmon resonance of the films are red-shifted as compared to non-linked particles, and that the red shift correlates linearly with the spacer length. This effect has been denoted as *coupled plasmon resonance* and depends on the NP proximity that is determined by the ligand. [6,8]

The effect of the ligand and the close proximity on the ensemble properties have as well been shown concerning the electrical properties of ligand-linked NPs. [8,101,102] Even for metallic NPs, the interparticle electric conductivity depends on the ligands: The conductivity of alkyl-linked NPs is dominated by the isolating character of the alkyl chains, so that interparticle electric conductivity occurs via core-to-core tunneling. [95] Consequently, the electric conductivity decreases with an increasing chain length due to the required activated electron hopping mechanism, but increases with increasing particle sizes (smaller particles have larger electronic band gaps and a smaller volume to interface ratio). The conductivity shows linear Arrhenius activation behavior and can be increased with increasing temperature. [70,101] In contrast, linking with an aromatic spacer enables electron transfer throughout the electric conducting linker and consequently enhances the interparticle electric conductivity compared to an alkyl spacer. [71,72,102]

However, the preparation of catalytic materials by ligand-linking has not been reported so far. Fig. 7.1 displays the linking ligands used in this work, which all consist of a hydrocarbon spacer, *e.g.* an alkyl chain or phenyl ring, and two amine head groups in $\alpha,\omega$- or *para*-position, respectively. The primary amines 1,8-diaminooctane (DAO) and *para*-phenylenediamine (PDA) have an alkyl or aryl spacer, respectively, and consequently differ in their conformational degrees of freedom and chemical stability of the backbone, while the hybridization of the amine group is similar. In contrast, 4,4'-bipyridine (BiPy) is a tertiary amine with the N incorporated in the aromatic system, which leads to a $sp^2$ hybridization of N. Consequently, the electron density is more localized at N as compared to the primary $sp^3$ amine of DAO and PDA. In addition, BiPy has little conformational degrees of freedom due to the aromatic sub-units.

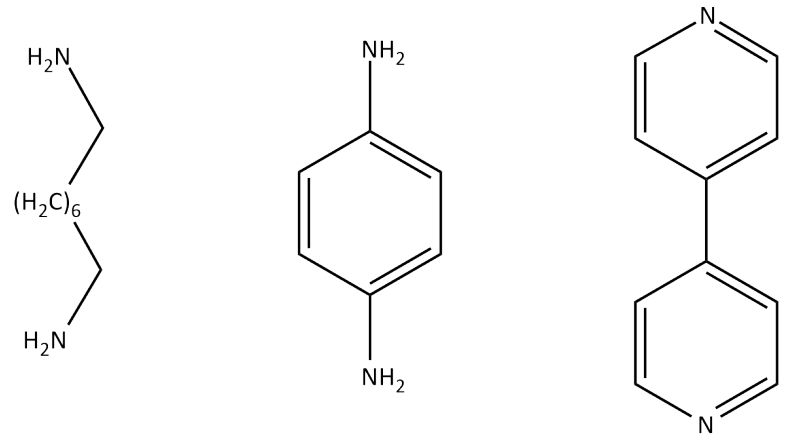


**Figure (7.1)** – *Structural formula of the bifunctional amines used for ligand-linking.*

The approach used for linking starts with "unprotected" Pt NPs, as sketched in Fig. 7.2. Both amine head groups of one ligand can bind to two individual NPs to link them (Fig. 7.2, middle). The linked NPs are, as a result, kept at a distance by the ligand. With proceeding linking, a three-dimensional network of NPs interconnected by bifunctional ligands is created (right sketch). Upon mixing a dispersion of "unprotected" NPs with a bifunctional ligand solution, the NPs will be linked and subsequently precipitate. A colorless solvent indicates successful incorporation of all NPs into the network. The

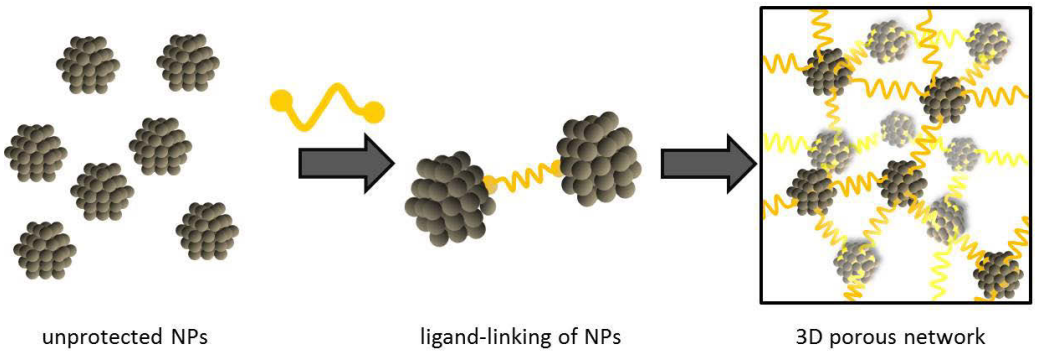


**Figure (7.2)** – *Ligand-linking: NPs are functionalized with bifunctional ligands that keep the NPs at a distance. As a result, agglomeration of the NPs is prevented. With proceeding functionalization three-dimensional ligand-stabilized NP networks are created.*

ligand-linking of Pt NPs with amines is not reversible and the ligand-linked NP networks are not soluble due to the anchoring of amines on Pt, as indicated by the precipitation. [8] In contrast to phase transfer reactions, functionalization with bifunctional ligands consequently has the advantage of a strong driving force toward the linked (adsorbed) state. A different type of cross-linking that has been reported occurs via hydrogen bridge bonding between ligand tails (Au-S-*spacer*-carboxyl $\cdots$ carboxyl-*spacer*-S-Au). This process however is reversible, as the networks can be dissolved in polar solvents. [8] As ligands with S-*spacer*-COOH functionality exhibit only one anchoring group (functional group to bind to the Au NP surface), they differ from the denotation of "bifunctional" ligands in this work.

So far, no detailed investigations about the mechanism of ligand-linking have been reported in literature. [103, 104] Mainly, two mechanisms are conceivable, which are sketched in Fig. 7.3. The first mechanism proposes that one NP will be densely covered by ligands, comparable to the functionalization with mono-amines. Subsequently, the ligands anchored on the first NP will cross-link unfunctionalized NPs with their second head group until all NPs are linked by ligands. A cross-linked network that precipitates is hence formed. The second mechanism proposes the first head group of one ligand binding to the first NP, while the second head group of this ligand binds to a different NP. A second ligand will bind with one head group to an already linked particle, while its second head group would link a third NP, and so forth. When the linked network has achieved a critical size, the network will precipitate and

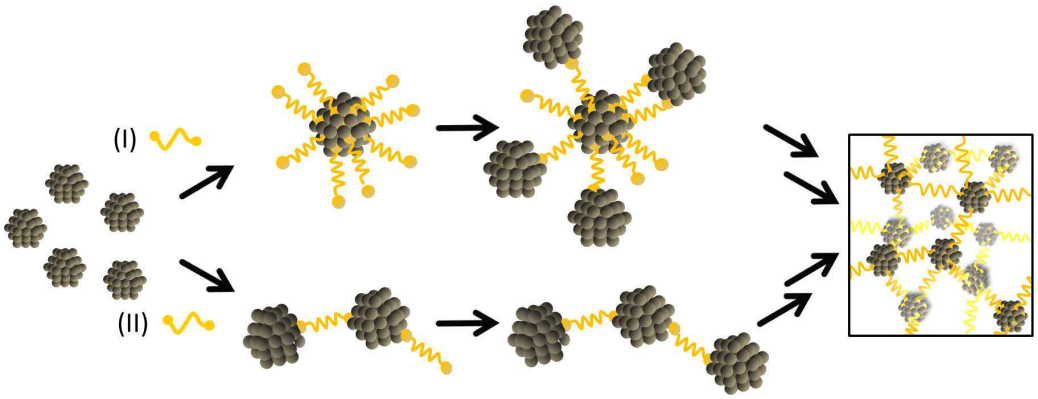


**Figure (7.3)** – *Two possible mechanisms for the ligand-linking of NPs. The first mechanism starts with functionalization of one NP similar to the binding of monofunctional ligands. Subsequently, the free head groups of the bound ligands cross-link unprotected NPs until a three-dimensional network is formed. The second mechanism may start with molecular linkage of one ligand between two NPs. Subsequently, the next unbound ligand will bind to a linked NP and, consequently, link another unprotected NP to the network.*

further growth or cross-linking will be inhibited. [103] However, it may be assumed that both pathways present borderline cases and that the actual linking mechanism is a combination of both. To distinguish between the two pathways, a tool for *in situ* characterization of the coverage or state of binding for individual NPs or ligands, respectively, would be necessary. Due to the fact that the linking is completed within short time frames, the mechanism could not be investigated yet.

## 7.2 Characterization of ligand-linked Pt NPs

The ligand-linked NPs are characterized in terms of ligand coverage, morphology of multilayer assemblies, and accessibility of surface sites. The results are compared with mono-amine functionalized NPs described in Chapter 3.

The linking can be performed by mixing "unprotected" Pt NPs with the diamine solution, as sketched in Fig. 7.2. The corresponding IR spectra are presented in Fig. 7.4 (left). The spectra of unfunctionalized Pt NPs has already been discussed in Chapter 2. The IR spectrum of PDA-Pt NPs reveals the diagnostic features of the ligand PDA, namely the $NH_2$ scissoring and aromatic C=C strechting vibrations between 1400–1600 $cm^{-1}$, confirming the successful

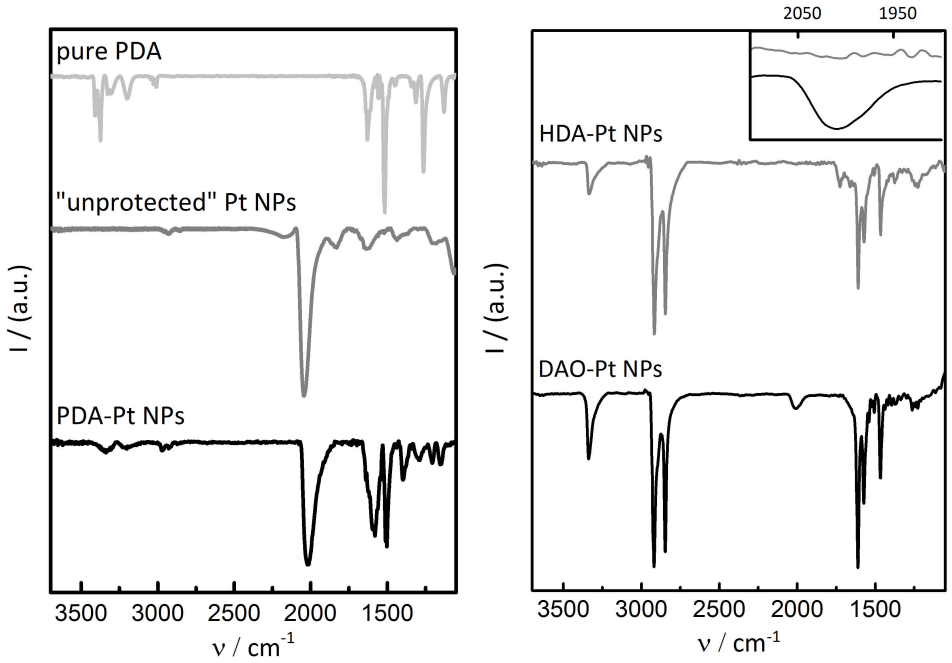


**Figure (7.4)** – *IR spectra following ligand-linking. Left: Ligand-linked Pt NPs (PDA-Pt) prepared from "unprotected" NPs with PDA. Right: Ligand-linked Pt NPs (DAO-Pt) prepared from mono-amine functionalized NPs (HDA-Pt) with DAO.*

NP functionalization. The decreased intensity of the $NH_2$ and aromatic C-H strechting vibrations ($\nu > 3000$ cm$^{-1}$) may be caused by anchoring of the amine ligand to the NP surface. After preparation, CO is adsorbed on the surface atoms of ligand-linked NPs, as indicated by the vibration around 2000 cm$^{-1}$, which evidences the presence of ligand-free surface sites.

In order to investigate the reason for the ligand-free surface sites, ligand-linking was performed starting from functionalized NPs. Fig. 7.4 (right) presents the spectrum of mono-amine functionalized HDA-Pt NPs that are subsequently exposed to DAO as a bifunctional ligand. Ligand-linked NP networks (DAO-Pt) are consequently formed via ligand exchange. As HDA and DAO have the same functional group, an equilibrium between binding of both ligands can be expected upon addition of the diamine to HDA-Pt NPs. However, the process of linking, which leads to the formation of an insoluble product, forces the equilibrium toward functionalization with the diamine (formation of DAO-Pt). The starting material HDA-Pt NPs is completely covered with the mono-functional amine, as indicated by the absence of CO

covered surface sites (see inset of Fig. 7.4, right). The resulting ligand-linked NPs of DAO-Pt show the vibration of adsorbed CO, which indicates the formation of ligand-free surface sites upon linking by desorption of HDA, see inset of Fig. 7.4. (For further discussion on the IR vibrations, the reader is referred to Publication [III].) The presence of ligand-free surface sites reveals that a full surface coverage with diamines is prevented. Fig. 7.5 sketches the geometric restrictions of cross-linking like limited conformational degrees of freedom within the ligand molecules and steric demands that may prevent full coverage. As a result, ligand-free surface sites are even created upon linking completely covered HDA-Pt NPs, which promises accessibility of surface atoms for catalytic reactions.

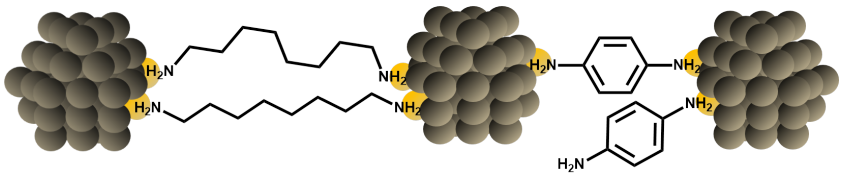


**Figure (7.5)** – *Ligand-linking of NPs with DAO and PDA. The restrictions concerning the conformational degrees of freedom prevent a complete coverage of the NP surface.*

If multilayer NP assemblies are used for catalytic applications, not only the presence of ligand-free surface sites of individual NPs is relevant. In addition, the accessibility of the sites is a relevant factor as diffusion limitations can lower the catalytic performance. The morphology of the ligand-linked Pt NPs was hence investigated. The three-dimensional assembly of ligand-linked particles sketched in Fig. 7.2 can be visualized by scanning electron microscopy (SEM). Fig. 7.6 displays SEM images of different ligand-linked NP networks. As the linking ligands are similar in terms of spacer length and head groups, no significant differences concerning the three-dimensional assembly and porous structure are found for the different diamines. A high magnification image of PDA-Pt enables the resolution of individual NPs (bright spots), which verifies that the porous assembly does not consist of sintered NPs. The porous assembly is in sharp contrast to the flat morphology of HDA-Pt NPs, as visualized in Fig. 4.3.

The accessibility of the catalytic component that is determined by the porosity can be verified by determining the specific surface area (surface area per mass) for different sample sizes. In a porous system with unrestricted accessibility to all layers (no diffusion limitations), the specific surface area should be

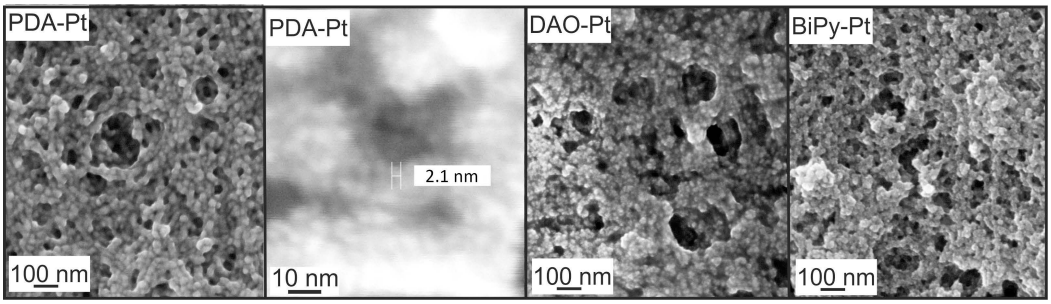


**Figure (7.6)** – *SEM images of ligand-linked Pt NP networks. Independent from the ligand, the NP networks all form a porous morphology. The high magnification image of PDA-Pt shows resolution of individual NPs (bright spots).*

independent from the sample size. As the specific surface area was determined electrochemically (by adsorption and desorption of hydrogen), the sample size equals the electrode loading. Fig. 7.7 displays the specific surface area (ECSA) of PDA-Pt for different electrode loadings. Within the uncertainty

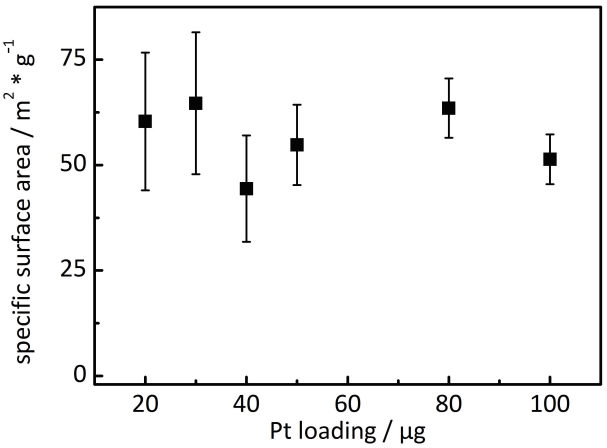


**Figure (7.7)** – *Specific surface area (ECSA) of PDA-Pt for different sample sizes determined by hydrogen under potential deposition ($H_{UPD}$). For a porous system, all layers should be accessible for the reactants which should result in a constant specific surface area for different sample sizes.*

of the measurement, the specific surface area remains constant for different sample sizes. These results demonstrate that ligand-linked NPs build a porous network with ligand-free surface sites that are accessible for catalytic reactions. As the pore size is determined by the spacer length of the ligands, however,

the accessibility of the porous structure may be limited when reactants of larger sizes are applied.

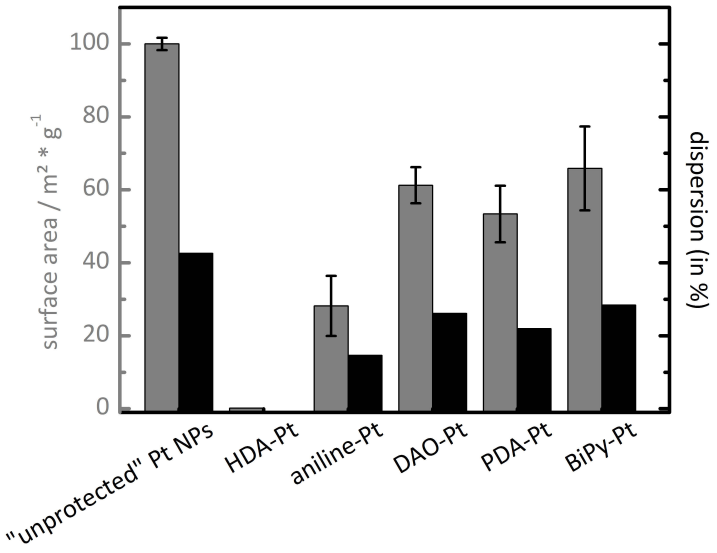


**Figure (7.8)** – *Absolute electrochemical surface area (grey) and dispersion (ratio of accessible surface sites to total number of Pt atoms per NP, black) of ligand-linked NPs determined by $H_{UPD}$.*

To determine the ratio of ligand-free surface atoms to the overall number of atoms (dispersion), the ECSA was correlated with NP sizes measured by TEM. The results and the comparison with values of mono-amine functionalized Pt NPs are shown in Fig. 7.8. The dispersion and ECSA of ligand-linked NPs are higher as compared to mono-functionalized Pt NPs, confirming the presence of free surface sites that are accessible for catalytic reactions. Interestingly, within the uncertainty of the experiments all NP networks of this study have the same free surface area irrespective of the ligand structure. The ECSA of ligand-linked NPs is about half of that of the unsupported and "unprotected" Pt NPs, due to the presence of surface bound ligands. The smaller amount of ligand-free surface sites may result in less reactant conversion per time as compared to "unprotected" NPs. However, as "unprotected" NPs undergo fast sintering due to the absence of any stabilization, there is a trade-off between the free surface area and blocking of surface sites required for particle stabilization.

For NPs stabilized on an inorganic support, the NP loading and, consequently, the number of active sites, is limited (ca. 1–10 wt% metal loading), as sintering

**Table (7.1)** – *Ratio of ligand molecules per Pt surface atoms for different ligand-linked NPs. The values have been determined by AAS/EA. The mono-functional ligand aniline was included, being a representative of a ligand without the possibility to cross-link two NPs such that the ligand coverage is only determined by its steric demands.*

| | aniline-Pt | PDA-Pt | DAO-Pt | BiPy-Pt |
|---|---|---|---|---|
| ligands per surface atom | 0.92 | 0.74 | 0.52 | 0.67 |

of the NPs cannot be prevented effectively at higher loadings. [9] To determine the weight ratio between Pt and ligands for ligand-linked NPs, AAS/EA measurements were performed. It was found that ligand-linked NPs consist of 71–73 wt% Pt (depending on the ligand), while the remaining ca. 30 wt% consist of the ligands and residual organic impurities. The ligand coverage can be found in Table 7.1 and can be correlated to the dispersion determined electrochemically (Fig. 7.8). In comparison to mono-functional amines, *e.g.* aniline, the ligand coverage with bifunctional ligands was found to be lower, which is in accordance with the higher ECSA. However, although the ECSA of different ligand-linked NPs can be considered equal, the number of ligand molecules per surface atom varies significantly between PDA, DAO, and BiPy, see Table 7.1.

As visualized in Fig. 7.5, due to geometrical and conformational restrictions not every bifunctional ligand can bind to two nanoparticles. A correlation between ECSA and ligand coverage allows for determining the degree of cross-linking ligands. A detailed derivation can be found in Publication [III]. The coverages with bifunctional ligands are compared to aniline-Pt, see Table 7.1, which represents a mono-functional ligand without the ability to cross-link, such that the coverage is merely determined by steric hindrance. It was found that DAO-Pt has the lowest number of ligand molecules per surface atom as compared to the investigated linking ligands. An alkyl chain as present in DAO can adopt different conformations. Fig. 7.5 illustrates how a high conformational flexibility of an alkyl chain allows for enhanced cross-linking of the NPs by the ligands. Thereby, one can correlate the low number of ligand molecules in DAO-Pt to a high degree of cross-linking. In comparison to DAO-Pt NPs, PDA-Pt and BiPy-Pt exhibit higher ligand contents. These results can be understood considering the more rigid structures of PDA and BiPy in comparison to the conformationally flexible structure of DAO. Consequently, the ability to cross-link two NPs decreases, as illustrated in Fig. 7.5, resulting in a higher ligand content in these samples.

A non-linking bifunctional ligand acts merely like a mono-functional ligand

in terms of stabilizing while blocking a surface atom. Thus, a high degree of cross-linking is desired, as it allows for an effective stabilization while keeping the number of blocked surface sites low. Consequently, a spacer with high conformational degrees of freedom, *e.g.* an alkyl chain, seems to be favorable over more rigid structures. However, as presented in Chapter 8, alkyl chains exhibit significant disadvantages in terms of stability as compared to aromatic structures. Thus, there is a compromise between the ability to crosslink and the chemical stability.

The presented ligand-linked NP networks are porous materials with free surface sites that are accessible for catalytic reactants. The approach of ligand-linking presents an alternative to catalytic NPs on inorganic supports. In addition, a high ratio between catalytically active sites and total catalyst mass, which is required for applications like catalytic gas sensing, is achieved, which qualifies ligand-linked NPs *e.g.* as promising candidates for gas sensing applications.

# 8 Gas sensing with ligand-linked NP catalysts

In this chapter, the catalytic potential of ligand-linked NPs is discussed based on their performance in hydrogen sensing and compared with the results of mono-amine functionalized Pt NPs.

The sensor and its working principle was already described in Chapter 5. Analog to Chapter 6, the sensors were exposed to a constant stream of $H_2$ in synthetic air, and the sensor output as a measure for the catalytic conversion of $H_2$ was recorded. Due to the fact that every sensor has been exposed to the same operating conditions (*e.g.* partial pressure of 1 vol% $H_2$), the different output signals can be correlated to different sensitivities of the catalysts. The output of different catalysts, converted to the generated temperature difference $\Delta T$, is displayed in Fig. 8.1 (left).

The time to achieve the maximum output displayed in the left graph is denoted as activation time and can be found in Fig. 8.1 (right). As shown in the IR spectra of as-prepared ligand-linked NPs (see for example Fig. 7.4), the ligand-free surface sites are initially covered with CO. To enable catalytic reactions, the surface sites have to be cleaned from these preparation residues. This activation phase lasts around 2.5 h irrespective of the linking ligand, which can be expected from the similar surface coverage of the NPs after preparation. However, compared to mono-amine functionalized Pt NPs, the activation phase of ligand-linked NPs was shorter, which can be explained by their surface coverage after preparation: The surface atoms of ligand-linked NPs are mainly covered with the amine ligands as stabilizers, while the ligand-free surface sites are covered by CO. To achieve the catalytic conversions, uncovered surface sites have to be created by desorption of either the ligands or CO. In comparison to amines, CO is a weaker adsorbate on Pt. [99, 100] This enables the desorption of CO during the activation phase, while the amines mainly remain adsorbed on the surface. The desorbed CO passes into the gas phase and is removed from the reactor. In this way, the surface atoms become accessible for catalytic reactions and the activity for hydrogen oxidation is established, while the stabilization by ligand functionalization

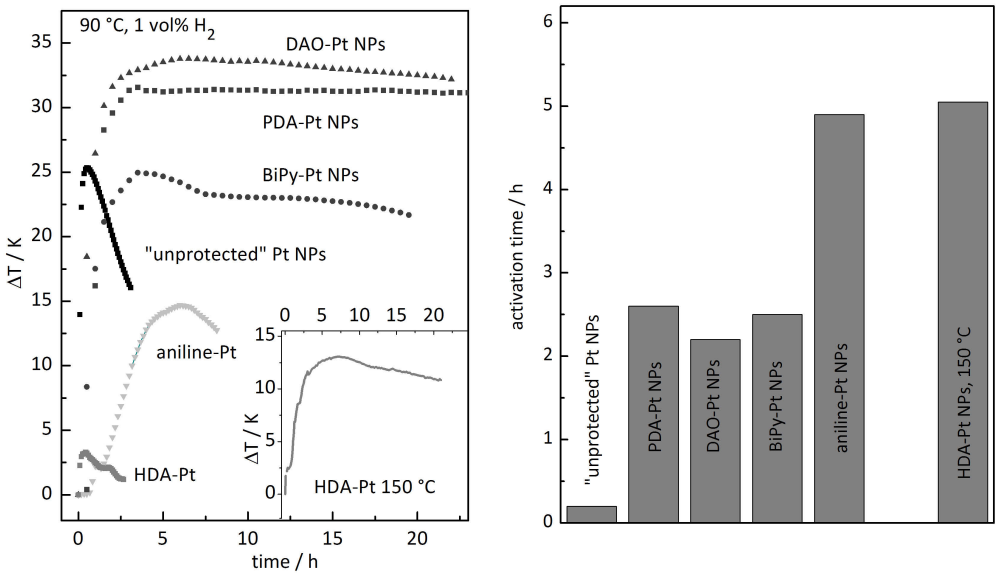


**Figure (8.1)** – *Sensor performance of functionalized NP catalysts. Left: Sensor output under a constant stream of hydrogen at 90 °C for different NP catalysts. The inset displays the output of HDA-Pt at 150 °C operating temperature. Right: Activation phase for the different catalysts to achieve maximum output.*

is maintained. For a more detailed description of the activation process, see Publication [IV].

After the activation phase, the output signal of BiPy-Pt and DAO-Pt slowly decreases over the course of the experiment, while the performance for PDA-Pt remains constant once the maximum activity is reached. The loss of activity of ligand-linked NPs occurs with a slower rate compared to aniline-Pt and HDA-Pt NPs.

As discussed for the sensor deterioration in Chapter 6, the stabilizing effect of ligands is only maintained in the adsorbed state and with intact ligands. Fig. 8.2 a) sketches the effects of partial ligand desorption on the NP stabilization for monofunctional amines during catalytic applications. The ligands may partially desorb from the NP surface under catalytic conditions (middle sketch). In the desorbed state, the ligands are free to depart from the vicinity of the NP surface (right sketch) or may even get decomposed. Consequently, re-adsorption is unlikely to occur once the ligands are desorbed from the NP and is prevented when the ligands are decomposed, which, in turn, diminishes the stabilizing effect on the NPs and enables sintering.

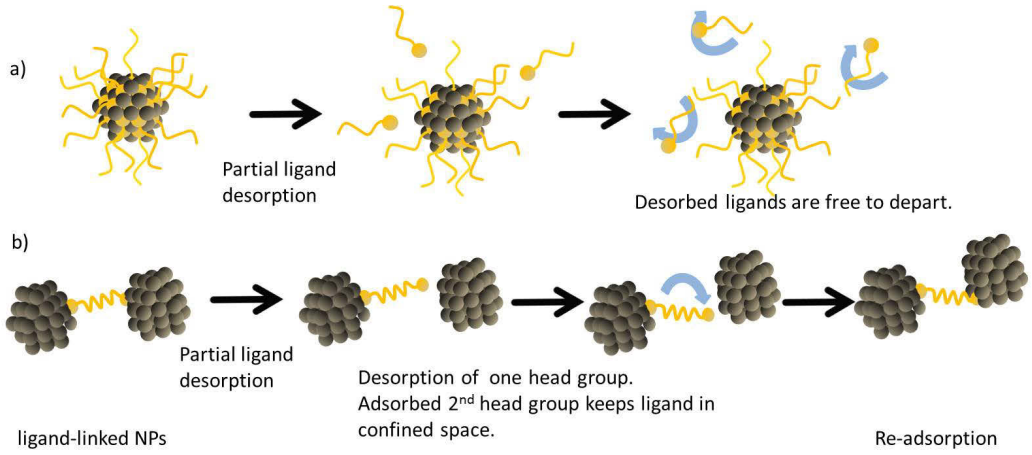


**Figure (8.2)** – *Partial ligand desorption of amines on Pt NPs. In the desorbed state, the stabilization effect on the NPs is diminished and the ligands may be decomposed in catalytic applications, which enables NP sintering. For mono-amines, re-adsorption of desorbed ligands is made difficult due to the fact that ligands may depart from the vicinity of the NPs. In contrast, the bifunctionality may support re-adsorption of desorbed head groups, as the second anchoring group and conformational restrictions leave the desorbed head group in the vicinity of the NP which, in turn, enables re-adsorption. As a result, the NPs are effectively stabilized.*

In contrast, for ligand-linked NPs partial amine desorption has a less negative impact, as illustrated in Fig. 8.2 b). An amine group may eventually desorb from the NP surface as well. However, when one head group of a bifunctional ligand is desorbed, the ligand is still anchored on a NP via its second head group. Movements of the anchored ligand are restricted by and limited to the intramolecular conformational degrees of freedom (see step 3). As a consequence of the anchoring, the ligand cannot depart the vicinity of the NP and the desorbed head group is restricted to a confined volume close to the NP surface. A re-adsorption of the desorbed head group is hence promoted, which leads to maintainance of the stabilization and prevents ligand decomposition. As the simultaneous desorption of both head groups of one ligand molecule is unlikely to occur, linking ligands can be considered as more effective NP stabilizers in comparison to mono-functional amines. However, differences in the stability of the sensor output can be found for different linking ligands. BiPy-Pt generates the lowest sensor output that additionally shows a drop in sensitivity after achieving the maximum. This decline can be explained by the $sp^2$ hybridization of the amines in BiPy,

as its binding strength to Pt is weaker as that of a $sp^3$ hybridized amine. The weaker binding strength encourages partial desorption of the BiPy head groups. In the desorbed state of BiPy, Pt is able to cleave the C-C bond between the pyridine sub-unites. [105] The bond cleavage and degradation of bipyridine to mono-functional pyridine units was identified with the help of IR spectroscopy before and after catalytic application (Fig. 8.3). (For a more detailed discussion of the IR study, see Publication [IV].) As a result, the stabilization effect due to the bifunctionality is reversed, which may lead to NP sintering, and, consequently, to a deteriorated sensor output.

The maximum sensitivity for DAO-Pt is similar to the one of PDA-Pt. However, the sensor output of DAO-Pt slowly decreases after reaching the maximum. IR spectroscopy (see Fig. 8.3 and Publication [IV]) revealed a cleavage of the amine group and oxidation of the alkyl chains during hydrogen sensing similar to HDA, which results in a loss of stabilization and degradation of the catalyst surface area.

In contrast, PDA-Pt generates a constant sensor output in a continuous stream of hydrogen. PDA ligand on Pt may partially desorb as well, which challenges the stability. However, the rigid conformation of PDA may effectively support re-adsorption of desorbed head groups as sketched in Fig. 8.2. Additionally, the aromatic backbone of PDA is chemically stable and is, thus, neither oxidized nor cleaved under the applied catalytic conditions (see Fig. 8.3). As a result, the NPs are stabilized and sintering is prevented, such that no catalyst degradation was observed for more than 20 h. The combination of a diamine and aromatic backbone as in PDA enables to stabilize NPs and create an active catalyst for hydrogen sensing. These results underline the great potential of ligand-linking for NP stabilization in catalytic sensing applications.

To summarize, the potential of ligand-linked Pt NPs as catalytic material was tested in a thermoelectric hydrogen sensor. The high density of active sites at a low catalyst weight allowed for a very short response time and a high sensitivity of the sensor. PDA-Pt remained active for more than 20 h on stream and produced a constant output signal. This performance can be attributed to the fact that the ligand remains intact and, hence, stabilizes the NPs.

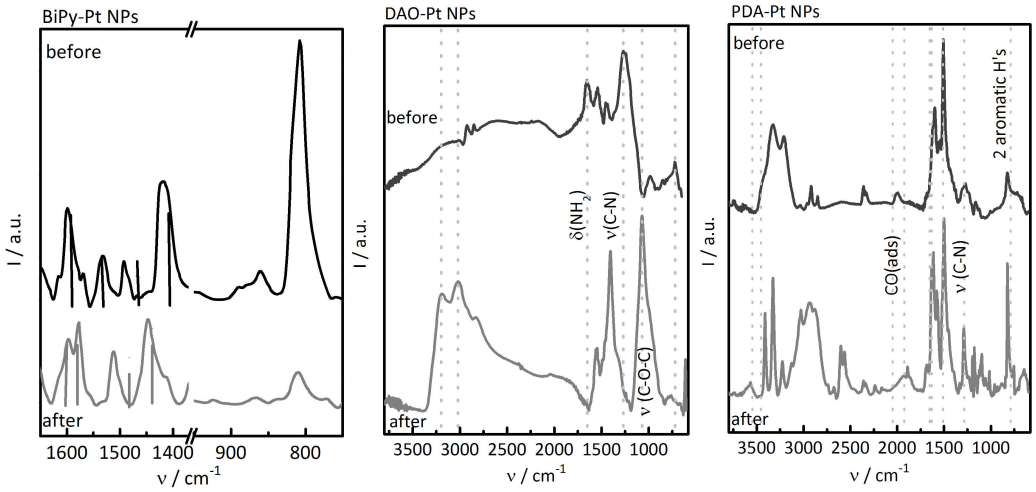


**Figure (8.3)** – *Reflection-IR spectra before and after $H_2$ oxidation experiments for different ligand-linked NP catalysts. The lines in the spectrum of BiPy-Pt before and after $H_2$ oxidation experiments mark vibrations of 4,4'-bipyridine and pyridine reference spectra, respectively. Comparison with the reference spectra indicate that the aromatic substructure is maintained during sensing, but the BiPy structure is cleaved into pyridine units which results the stabilization effect of a mono-functional ligand. The vibration at ∼800 $cm^{-1}$ is assigned to the deformation vibration of two neighbored aromatic H's, which is diminished upon bond cleavage between the pyridine units.*
*For DAO-Pt, the $NH_2$ deformation vibration as well as the C-N vibration vanished after the sensing, which indicates the cleavage and destruction of the amine groups. A very distinct vibration that is assigned to a C-O-C strechting vibration as well as two vibrations $\nu > 3000$ $cm^{-1}$ arose, which indicate the formation of epoxides by oxidation of the alkyl chain. As a result, the stabilization effect is diminished.*
*For PDA-Pt, after the $H_2$ oxidation experiments the adsorbed CO vanished, indicating the cleaning of ligand-free surface atoms during the activation phase. In addition, in the post-oxidation spectrum the diagnostic vibrations to identify aromatic compounds and primary amines are still present. This fact indicates that the PDA structure is stable over the course of the catalytic experiment.*

# 9 Ligand-linked NPs in electrochemistry

The catalytic potential of ligand-linked NPs was shown above with their application in a gas sensor, where the high density of active sites and the stability of PDA-Pt enabled a good sensor performance. Other applications of catalytic NPs, for example mobile fuel cells, also require a high density of active sites at low overall catalyst mass for *e.g.* achieving a high current density per catalyst mass. [106, 107] The most common choice of electrocatalysts are Pt and Pt alloy NPs supported on high surface area carbon. [66, 107] In contrast to oxide supports like $Al_2O_3$, carbon facilitates electric conductivity and allows for a higher catalyst loading due to its enormous achievable surface areas and its low molecular weight. [108] Due to the fact that a high number of electrochemically accessible surface sites were found for ligand-linked Pt NPs, one may speculate about the potential of ligand-linked NPs as electrocatalysts. This chapter will be an excursus considering the properties and the stability of PDA-Pt NPs during cyclic voltammetry (CV).

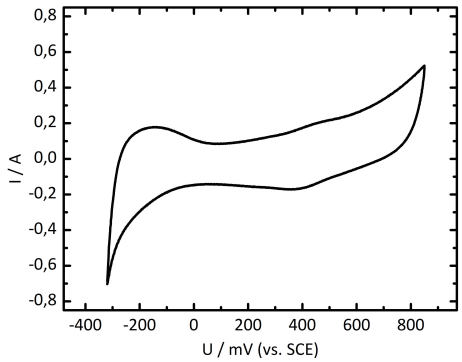


**Figure (9.1)** – *Cyclic voltammogram of PDA-Pt NPs. The sample of PDA-Pt NPs has been applied onto the glassy carbon electrode without external support or fixation. The peaks visible in the CV correspond to the features of Pt, namely hydrogen adsorption and desorption as well as the formation and reduction of an oxygenated Pt species.*

The CV of PDA-Pt is displayed in Fig. 9.1 and reveals the characteristic peaks of a Pt surface, like hydrogen adsorption and desorption peaks (U < 0 mV) or the reversible formation and reduction of oxygenated Pt species (around 400 mV). These results indicate that ligand-linked NPs provide ligand-free surface sites that are accessible for electrochemical reactions.

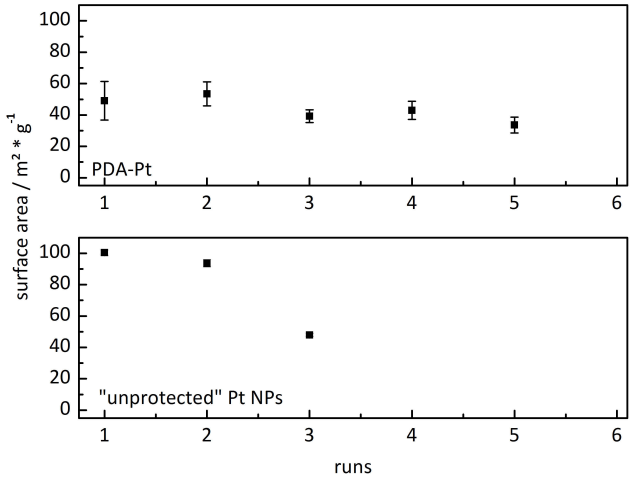


**Figure (9.2)** – *Development of the surface area of "unprotected" Pt NPs and PDA-Pt over repeated CV runs. Each "run" consists of about 30 potential cycles. For "unprotected" NPs, the error bars were smaller than the dimensions of the data points. Due to the fact that "unprotected" NPs show a sharp surface decrease, no further runs were performed.*

Fig. 9.2 presents the development of the surface area of "unprotected" Pt NPs and PDA-Pt NPs over several runs of CV measurements, with each run consisting of about 30 potential cycles. Further comparison with the stability of mono-amine functionalized NPs are omitted due to their small surface area. As described in the previous chapter adressing the NP stabilization, unsupported and "unprotected" Pt NPs showed an ECSA of about 100 $m^2/g$. Due to their missing stabilization, the surface area of "unprotected" Pt NPs rapidly diminished over the course of the experiment. For PDA-Pt an ECSA of around 53 $m^2/g$ (corresponds to a dispersion of 0.25, see Fig. 7.8) was determined and the accessibility of the whole sample without diffusion limitations (Fig. 7.7) was confirmed in Chapter 7. In contrast to "unprotected" NPs, the surface of PDA-Pt showed no significant decrease over repeated potential cycles (Fig. 9.2).

To evaluate the potential of ligand-linked NPs in electrocatalytic reactions further investigations are required. So far, it was demonstrated that sintering of NPs is successfully prevented by stabilization with PDA even under electrochemical conditions, and the surface area of the material is maintained.

# 10 Naphthylamine as participating ligand in electrochemistry

In this chapter, we introduce the system of 1-naphthylamine (napha) functionalized Pt NPs and the phenomenon of an aromatic ligand participating in electrochemical reactions. So far, the task of the ligands in this study was to stabilize NPs. However, we found that functionalization with mono-amines does not allow for the formation of stable and active sensor catalysts. When the NPs are supported, the ligands may change their task from being a passive stabilizer (spectator) to becoming an active participant in catalytic reactions. For example, Kahsar *et al.* reported that organic ligands on Pt NPs direct the orientation of reactant molecules during adsorption on Pt surface sites and thereby increase the chemo-selectivity in hydrogenation reactions. [109]

Aromatics may be suitable as participating ligands in electrochemical applications due to their ability to perform reversible redox reactions. Aromatic ligands bound to Pt NPs are expected to form a conjugated system where the molecular orbitals of the hydrocarbon backbone, amine head group, and metal NP overlap so that charge can be transferred between metal particle and aromatic system. [72] If their redox behavior was maintained upon functionalization to Pt NPs, a system may be created where the ligands can undertake an active role during potential cycles. A material may hence be generated which combines the functionality of an organic molecule and a catalytic metal. Even synergistic effects between ligand and metal may be possible.

1-Naphthylamine is a mono-functional amine with acquainted redox behavior. Electrochemically induced, the aromatic system of 1-naphthylamine can form stable radical cations with the charge being delocalized over the aromatic system. [110, 111] The CV of freshly prepared napha-Pt NPs supported on carbon presented in Fig. 10.1 shows a reversible redox peak that is assigned to a redox reaction of the ligand. This result demonstrates that the redox behavior of the aromatic system is maintained upon binding to Pt NPs and that the charge can be transferred across the amine head group. A correlation between

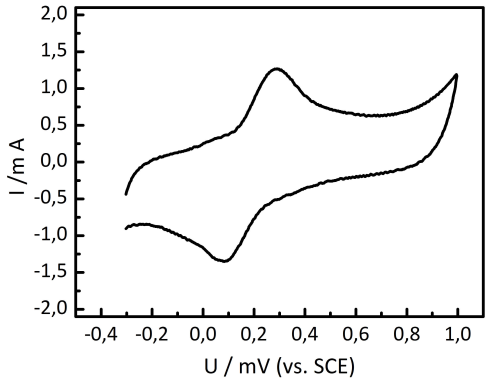


**Figure (10.1)** – *Cyclic voltamogramm of freshly prepared Napha-Pt NPs supported on carbon. The material shows a reversible redox peak that is assigned to a redox reaction of the ligand.*

ligand coverage (determined via EA/AAS) and transferred charge (determined by peak integration of the CV) reveals that the observed redox reaction is a one-electron-transfer that forms a stable radical cation of naphthylamine. Although IR spectroscopy revealed the presence of ligand-free surface sites, no features of Pt are found in the CV. In addition, the CV does not reveal a CO stripping peak, so that no electrocatalytic activity was found for freshly prepared napha-Pt NPs. For electrocatalytic reactions like CO stripping, the presence of contiguous surface sites is prerequisite. However, the assignment of the IR vibrations indicated that the ligands are evenly distributed over the NP surface, so that no contiguous ligand-free surface sites are present. As a result, the electrocatalytic activity may be suppressed by the evenly distributed ligand shell. For a more detailed discussion about the IR vibrations and the inhibition of electrocatalytic reactions of covered surfaces, see Publication [VI].

A napha-Pt NP dispersion was kept without excess of unbound ligands in order to take advantage of the dynamic adsorption-desorption-equilibrium of amines on Pt to induce a partial ligand desorption. In this way, adjacent ligand-free surface sites may be generated and an electrocatalytic activity of the NPs may be enabled. After several days of aging, denoted as "catalytically activation", the identical CV procedure was performed with napha-Pt NPs. The resulting CVs are displayed in Fig. 10.2. As expected, two oxidation peaks occur. The ligand redox peak is maintained, and additionally CO stripping can be performed at the Pt surface.

For the creation of accessible Pt ensembles different mechanisms may be

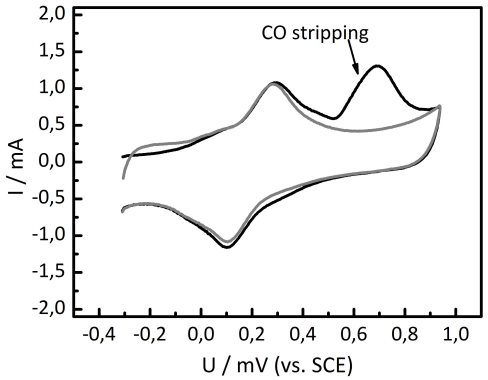


**Figure (10.2)** – *Cyclic voltamogramm of catalytically activated Napha-Pt NPs. The ligand redox peak is maintained. Additionally, CO stripping was enabled.*

feasible. Either the ligands may partially desorb during the aging, or the ligand shell may re-arrange to result in ensembles of ligand-free Pt sites. For aromatic ligands, a re-arrangement on surfaces and even NPs into "island" have been reported, which are induced by strong intermolecular attraction. [112, 113] As aromatic systems like in naphthylamine experience strong $\pi$-$\pi$ attraction, [85, 114] it may even be possible that the amine groups partially desorb from the NP surface, while the ligand remains within the ligand shell by the formation of $\pi$-$\pi$ dimers or stacks. In order to elucidate the activation process, different characterizations were performed, namely IR-spectroscopy, NMR-spectroscopy, EA/AAS. No indications for desorbed ligands were found, so that a removal of ligands from the ligand shell can be excluded. Consequently, a re-arrangement of the ligand shell during the aging is proposed in order to enable the formation of catalytically active Pt ensembles. However, the re-arrangement of the ligands is not accessible with standard characterization techniques. For further details about the proposed mechanism for the re-arrangement, see Publication [VI].

To summarize, napha-Pt NPs not only represents a system where the organic ligand is stable under electrocatalytic conditions, but also performs redox reactions. In addition, the Pt surface sites of napha-Pt can be activated for electrocatalytic reactions. Hence, a hybrid material is created that allows for simultaneous electrochemical reaction on the metal surface and its organic ligand. These results show that the role of ligands is not limited to being a spectator, but they can participate in electrochemical reactions.

# 11 Conclusion and Outlook

Nanoparticles (NPs) are known to exhibit unique chemical and physical properties in comparison to the corresponding bulk materials. Due to their large surface-to-volume ratio and the resulting high surface energy, nanoparticles tend to aggregate and coalesce, which results in a loss of the nano-structure. Stabilization of NPs is hence prerequisite for any application in order to maintain the specific properties of nanoscaled materials. Different approaches toward stabilization of nanoparticles can be found in the literature. For example, the state-of-the-art stabilization for NPs in heterogeneous catalysis is to support them onto inert inorganic materials (*e.g.* $Al_2O_3$). Thereby, stabilization is achieved by dispersing the NPs over the surface of the support. As the particles may become mobile under catalytic conditions, this approach is limited to low loadings of the catalytically active material to ensure the stabilization. However, applications such as thermoelectric gas sensing require a high density of catalytically active sites at a low total heat capacity in order to achieve a short response time and a strong sensor signal. Consequently, supported NPs exhibit significant limitations for applications that require a high density of the catalytically active component.

The aim of this work was to investigate the stabilization of catalytic NPs with organic ligands as an alternative approach to the supporting of NPs. The catalytic properties of such stabilized NPs was exemplary investigated by their application in a thermoelectric hydrogen sensor. To exclusively determine the influence of the ligand on the material properties, a synthetic protocol was applied which allows for the separation of NP synthesis and functionalization. The absence of strongly binding adsorbates during the synthesis produces so-called "unprotected" NPs and allows for an easy functionalization of the NPs with various ligands in a separate step. Mono- and diamines were applied as ligands in this study.

After preparation, Pt NPs stabilized with mono-amines were mostly covered with ligands (ligand coverages between 0.92 to 1). Investigation of their catalytic properties showed that the high ligand coverages almost completely suppresses the catalytic activity of the particles. Accessible surface sites can be generated *in situ* by partial ligand desorption, which, however, diminishes

the stabilization. As a result, the NPs may aggregate and the surface area of the catalyst decreases. In conclusion, mono-amines are not suitable for the stabilization of Pt NPs for catalytic applications. The catalytically active surface area is low due to the high ligand coverage, and the stabilization of NPs under catalytic conditions is insufficient.

The concept of molecular linkage of nanoparticles with bifunctional amine ligands (*ligand-linking*) was introduced as an alternative to the use of monofunctional ligands. It was found that amine-linked Pt NPs form three-dimensional porous networks with ligand-free surface sites that are accessible for catalytic reactions. After preparation, the ligand-free surface atoms are covered with CO, which desorbs during a catalytic activation phase. As a consequence, the ligand-free surface atoms are accessible for reactant adsorption and conversion, and high activities can be achieved. Compared to mono-amine stabilized NPs, the stability can be significantly improved by ligand-linking. One reason may be that during a possible desorption of one head group the bifunctional ligand remains anchored on a NP via the second head group. This anchoring can enhance re-adsorption of the desorbed head group, so that stabilization is maintained. The stabilizing effect of the ligands during catalytic applications, however, is only maintained as long as the ligands are intact. By examining the stability achieved by different ligand structures it was identified that an aromatic hydrocarbon skeleton is favored over an alkyl backbone. Furthermore, the presence of two head groups is required, and primary $sp^3$ hybridized amine groups allow for better stabilization than aromatic $sp^2$ hybridized amines due to their higher binding strength to Pt. These criteria are best met by *para*-phenylenediamine (PDA), so that by linking of Pt NPs with PDA a constant catalytic activity over more than 20 h on stream was reached. Thus, it could be shown that organic ligands can be successfully applied to stabilize catalytic NPs.

The application of the mono-amine 1-naphthylamine (napha) shows that ligands are not only able to stabilize catalytic NPs while being a passive "spectator", but can also take over an active role: Napha functionalized Pt NPs supported on carbon show a electrochemically induced reversible redox reaction of the ligand. After a pre-treatment, the Pt surface atoms can also be activatead for electrocatalytic reactions (*e.g.* CO stripping). Thus, napha-Pt not only demonstrates that an organic ligand is stable under electrocatalytic conditions, but in addition a hybrid material is formed with a parallel electrochemical reaction of the metal surface and the ligand.

**Outlook** Future studies on NP catalysts for gas sensing may investigate the implementation of selectivity toward gas mixtures by a sophisticated choice of the ligand. In addition to the stabilizing effect, the ligands direct the porosity of the NP network, as the minimum pore size is determined by the ligand spacer length and its steric demand. The diffusion of reactants into a porous system depends on the ratio of pore diameter to reactant size. In this way, by adjusting the porosity of the ligand-linked NP network, one may implement selectivity by inhibiting the diffusion of larger molecules into the particle network. Further improvements of the long-term stability by the application of different ligand structures may be achievable. Although PDA-Pt is stable over more than 20 h of catalytic activity, the $\sigma$-bond between amine group and aromatic system is a site of fracture. A ligand structure may be identified which enables a strong bond toward Pt but without internal sites of fractures.

A second pathway toward implementation of selectivity and improvements of the stability may be the application of bimetallic NPs. The decomposition of ligands during sensor operations is expected to be assisted by larger Pt ensembles. The alloying of Pt with a catalytically inactive metal could dilute Pt surface atoms and, in this way, decrease the size of Pt ensembles. The active surface area of bimetallic NPs may be maintained by selective ligand functionalization. For example, carboxylates are known to strongly bind to Ag or Sn, while no stable bond is formed to Pt. Thereby, ligand-linking of PtM NPs (M = Ag or Sn) with a bifunctional carboxylate ligand (*e.g.* terephthalic acid) could exclusively occur via carboxylate-M bonds and leave Pt surface atoms ligand-free. An alloying of the catalytic NPs may also result in a different electronic structure. Thereby, selective adsorption of gases may be achieved and a selective response toward one gas in a gas mixture could be implemented.

The application of ligand-stabilized and ligand-functionalized NPs in electrochemical applications may be investigated in more detail. The ensemble size plays an important role for electrocatalytic reactions as well, as almost all electrocatalytic reaction require adjacent Pt surface atoms. Consequently, the linking ligands should be chosen in a way that ligand-free Pt ensembles are created by the steric demands and intermolecular interactions of the ligand while maintaining the stabilization.

In addition, the interplay between 1-naphthylamine and Pt NPs in electrochemical reactions is an interesting starting point for further applications. Therefore, it should be investigated if not only a hybrid material with functionality on ligand and metal can be build, but furthermore whether synergistic effects may be achievable.

# Bibliography


[1] Shiju, N. R.; Guliants, V. V. *Appl Catal A-Gen* **2009**, *356*, 1–17.

[2] Goesmann, H.; Feldmann, C. *Angew. Chem. Int. Ed. Engl.* **2010**, *49*, 1362–1395.

[3] Wegner, K.; Pratsinis, S. E.; Köhler, M. In *Nanomaterialien und Nanotechnologie*; Winnacker/Küchle„ Ed.; Wiley-VCH: Weinheim, 2004; Vol. 2, pp 821–905.

[4] Schmid, G. *Nanoparticles*; Wiley-VCH: Weinheim, 2004.

[5] Rao, C. N. R.; Müller, A.; Cheetham, A. *The Chemistry of Nanomaterials*; Wiley-VCH: Weinheim, 2004.

[6] Shipway, A. N.; Katz, E.; Willner, I. *ChemPhysChem* **2000**, *1*, 18–52.

[7] Kawasaki, H.; Yamamoto, H.; Fujimori, H.; Arakawa, R.; Inada, M.; Iwasaki, Y. *Chem. Commun. (Camb)* **2010**, *46*, 3759–3761.

[8] Wang, L.; Luo, J.; Schadt, M. J.; Zhong, C. J. *Langmuir* **2010**, *26*, 618–632.

[9] Challa, S. R.; Delariva, A. T.; Hansen, T. W.; Helveg, S.; Sehested, J.; Hansen, P. L.; Garzon, F.; Datye, A. K. *J. Am. Chem. Soc.* **2011**, *133*, 20672–20675.

[10] Boon-Brett, L.; Bousek, J.; Black, G.; Moretto, P.; Castello, P.; Hübert, T.; Banach, U. *Int. J. Hydrogen Energy* **2010**, *35*, 373–384.

[11] Kocemba, I.; Rynkowski, J. *Sensors and Actuators B: Chemical* **2011**, *155*, 659–666.

[12] Ortiz, N.; Skrabalak, S. E. *Langmuir* **2014**, *30*, 6649–6659.

[13] Bass, J. D.; Ai, X.; Bagabas, A.; Rice, P. M.; Topuria, T.; Scott, J. C.; Alharbi, F. H.; Kim, H. C.; Song, Q.; Miller, R. D. *Angew. Chem. Int. Ed. Engl.* **2011**, *50*, 6538–6542.

[14] Burda, C.; Chen, X.; Radha, N.; El-Sayed, M. A. *Chem. Rev.* **2005**, *105*, 1025–1102.

[15] Peng, X. *Adv. Mater.* **2003**, *15*, 459–463.

[16] Krebs, R. E. In *Platinum*; Greenwood Press, 1998; pp 124–127.

[17] Jana, N. R.; Peng, X. *J. A. Chem. Soc.* **2003**, *125*, 14280–14281.

[18] Park, J.; Joo, J.; Kwon, S. G.; Jang, Y.; Hyeon, T. *Angew. Chem. Int. Ed. Engl.* **2007**, *46*, 4630–4660.

[19] Toshima, N.; Yonezawa, T. *New Journal of Chemistry* **1998**, *22*, 1179–1201.

[20] Ghosh, T.; Leonard, B. M.; Zhou, Q.; DiSalvo, F. J. *Chem. Mater.* **2010**, *22*, 2190–2202.

[21] Yu, Y.; Yang, W.; Sun, X.; Zhu, W.; Li, X. Z.; Sellmyer, D. J.; Sun, S. *Nano Lett.* **2014**, *14*, 2778–2782.

[22] Yuan, Q.; Wang, X. *Nanoscale* **2010**, *2*, 2328–2335.

[23] Viau, G.; Brayner, R.; Poul, L.; Chakroune, N.; Lacaze, E.; Fievet-Vincent, F.; Fievet, F. *Chem. Mater.* **2003**, *15*, 486–494.

[24] Yu, H.; Gibbons, P. C.; Kelton, K.; Buhro, W. E. *J. Am. Chem. Soc.* **2001**, *123*, 9198–9199.

[25] Zeng, H.; Sun, S. *Adv. Funct. Mater.* **2008**, *18*, 391–400.

[26] Selvakannan, P. R.; Sastry, M. *Chem. Commun. (Camb)* **2005**, 1684–1686.

[27] Auten, B. J.; Lang, H.; Chandler, B. D. *Applied Catalysis B: Environmental* **2008**, *81*, 225–235.

[28] Faraday, M. *Philos. Trans. R. Soc. London* **1857**, *147*, 147–153.

[29] LaMer, V. K.; Dinegar, R. H. *J. A. Chem. Soc.* **1950**, *72*, 4847–4854.

[30] Bönnemann, H.; Richards, R. M. *Eur. J. Inorg. Chem.* **2001**, 2455–2480.

[31] Biacchi, A. J.; Schaak, R. E. *ACS Nano* **2011**, *5*, 8089 – 8099.

[32] Chen, J.; Herricks, T.; Xia, Y. *Angew. Chem. Int. Ed. Engl.* **2005**, *44*, 2589–2592.

[33] Turkevich, J.; Stevenson, P.; Hillier, J. *Discussions of the faraday society* **1951**, 55–75.

[34] Mulvaney, P. In *Metal Nanoparticles: Double Layers, Optical Properties, and Electrochemistry*; Klabunde, K. J., Ed.; John Wiley and Sons, Inc., 2001; pp 121–167.

[35] Pileni, M.-P. *J. Phys. Chem.* **1993**, *97*, 6961–6973.

[36] Ingelsten, H. H.; Bagwe, R.; Palmqvist, A.; Skoglundh, M.; Svanberg, C.; Holmberg, K.; Shah, D. O. *J. Colloid Interface Sci.* **2001**, *241*, 104–111.

[37] Ingelsten, H. H.; Beziat, J.-C.; Bergkvist, K.; Palmqvist, A.; Skoglundh, M.; Qiuhong, H.; Falk, L. K.; Holmberg, K. *Langmuir* **2002**, *18*, 1811–1818.

[38] Wikander, K.; Petit, C.; Holmberg, K.; Pileni, M.-P. *Langmuir* **2006**, *22*, 4863–4868.

[39] Tadros, T. F. *Polymer Journal* **1991**, *23*, 683–696.

[40] Moreels, I.; Martins, J. C.; Hens, Z. *ChemPhysChem* **2006**, *7*, 1028–1031.

[41] Fu, X.; Wang, Y.; Wu, N.; Gui, L.; Tang, Y. *J. Colloid Interf. Sci.* **2001**, *243*, 326–330.

[42] Ryu, J. H.; Han, S. S.; Kim, D. H.; Henkelmann, G.; Lee, H. M. *ACS Nano* **2011**, *5*, 8515–8522.

[43] Johnson, S.; Evans, S.; Brydson, R. *Langmuir* **1998**, *14*, 6639–6647.

[44] Giersig, M.; Mulvaney, P. *Langmuir* **1993**, *9*, 3408–3413.

[45] Martin, J. E.; Wilcoxon, J. P.; Odinek, J.; Provencio, P. *J. Phys. Chem. B* **2002**, *106*, 971–978.

[46] Mourdikoudis, S.; Liz-Marzán, L. M. *Chem. Mater.* **2013**, *25*, 1465–1476.

[47] Wang, C.; Daimon, H.; Onodera, T.; Koda, T.; Sun, S. *Angew. Chem. Int. Ed. Engl.* **2008**, *47*, 3588–3591.

[48] Song, H.; Kim, F.; Connor, S.; Somorjai, G. A.; Peidong, Y. *J. Phys. Chem. B* **2005**, *109*, 188–193.

[49] Hirai, H.; Nakao, Y.; Toshima, N. *Chem. Lett.* **1978**, 545–548.

[50] Hirai, H.; Nakao, Y.; Toshima, N. *Journal of Macromolecular Science-Chemistry* **1978**, *A12*, 1117–1141.

[51] Hirai, H.; Nakao, Y.; Toshima, N. *Journal of Macromolecular Science-Chemistry* **1979**, *A13*, 727–750.

[52] Song, H.; Rioux, R. M.; Hoefelmeyer, J. D.; Komor, R.; Niesz, K.; Grass, M.; Yang, P.; Somorjai, G. A. *J. A. Chem. Soc.* **2006**, *128*, 3027–3037.

[53] Sato, T.; Ruch, R. *Stabilization of colloidal dispersions by polymer adsorption*; Surfactant Science Series; Marcel Dekker, Inc.: New York, 1980.

[54] Rioux, R. M.; Song, H.; Grass, M.; Habas, S.; Niesz, K.; Hoefelmeyer, J. D.; Yang, P.; Somorjai, G. A. *Top. Catal.* **2006**, *39*, 167–174.

[55] Koole, R.; Schapotschnikow, P.; de Mello Donegá, C.; Vlugt, T. J. H.; Meijerink, A. *ACS Nano* **2008**, *2*, 1703–1714.

[56] Moran, C. H.; Rycenga, M.; Zhang, Q.; Xia, Y. *J. Phys. Chem. C Nanomater Interfaces* **2011**, *115*, 21852–21857.

[57] Dong, A.; Ye, X.; Chen, J.; Kang, Y.; Gordon, T.; Kikkawa, J. M.; Murray, C. B. *J. Am. Chem. Soc.* **2011**, *133*, 998–1006.

[58] Feldmann, C.; Jungk, H.-O. *Angew. Chem. Int. Ed. Engl.* **2001**, *40*, 359–362.

[59] Feldmann, C. *Adv. Funct. Mater.* **2003**, *13*, 101–107.

[60] Fievet, F.; Lagier, J.; Blin, B. *Solid State Ionics* **1989**, *32/33*, 198–205.

[61] Wang, Y.; Ren, J.; Deng, K.; Gui, L.; Tang, Y. *Chem. Mater.* **2000**, *12*, 1622–1627.

[62] Bock, C.; Paquet, C.; Couillard, M.; Botton, G. A.; MacDougall, B. R. *J. Am. Chem. Soc.* **2004**, *126*, 8028–8037.

[63] Witte, P. T.; Berben, P. H.; Boland, S.; Boymans, E. H.; Vogt, D.; Geus, J. W.; Donkervoort, J. G. *Top. Catal.* **2012**, *55*, 505–511.

[64] Sonström, P.; Bäumer, M. *PhysChemChemPhys* **2011**, *13*, 19270.

[65] Meille, V. *Applied Catalysis A: General* **2006**, *315*, 1–17.

[66] Meier, J. C.; Galeano, C.; Katsounaros, I.; Witte, J.; Bongard, H. J.; Topalov, A. A.; Baldizzone, C.; Mezzavilla, S.; Schuth, F.; Mayrhofer, K. J. *Beilstein J. Nanotechnol.* **2014**, *5*, 44–67.

[67] Hanson, F. V.; Boudart, M. *J. Catal.* **1978**, *53*, 56–67.

[68] Korgel, B. A.; Fullam, S.; Conolly, S.; Fitzmaurice, D. *J. Phys. Chem. B* **1998**, *102*, 8379–8388.

[69] Lewandowski, W.; Jatczak, K.; Pociecha, D.; Mieczkowski, J. *Langmuir* **2013**, *29*, 3404–3410.

[70] Joseph, Y.; Besnard, I.; Rosenberger, M.; Guse, B.; Nothofer, H.-G.; Wessels, J. M.; Wild, U.; Knop-Gericke, A.; Su, D.; Schlögl, R.; Yasuda, A.; Vossmeyer, T. *J. Phys. Chem. B* **2003**, *107*, 7406–7413.

[71] Joseph, Y.; Peic, A.; Chen, X.; Michl, J.; Vossmeyer, T.; Yasuda, A. *J. Phys. Chem. C* **2007**, *111*, 12855–12859.

[72] Wessels, J. M.; Nothofer, H.-G.; Ford, W. E.; von Wrochem, F.; Scholz, F.; Vossmeyer, T.; Schroedter, A.; Weller, H.; Yasuda, A. *J. A. Chem. Soc.* **2004**, *126*, 3349–3356.

[73] Hiraishi, J.; Nakagawa, I.; Shimanouchi, T. *Spectrochim. Acta* **1968**, *24A*, 819–832.

[74] Love, J. C.; Estroff, L. A.; Kriebel, J. K.; Nuzzo, R. G.; Whitesides, G. M. *Chem. Rev.* **2005**, *105*, 1103–1169.

[75] Castro, E. G.; Salvatierra, R. V.; Schreiner, W. H.; Oliveira, M. M.; Zarbin, A. J. G. *Chem. Mater.* **2010**, *22*, 360–370.

[76] Miyabayashi, K.; Nishihara, H.; Miyake, M. *Langmuir* **2014**, *30*, 2936–2942.

[77] Yang, J.; Lee, J. Y.; Ying, J. Y. *Chem. Soc. Rev.* **2011**, *40*, 1672.

[78] Schladt, T. D.; Schneider, K.; Shukoor, M. I.; Natalio, F.; Bauer, H.; Tahir, M. N.; Weber, S.; Schreiber, L. M.; Schröder, H. C.; Müller, W. E. G.; Tremel, W. *J. Mater. Chem.* **2010**, *20*, 8297.

[79] Tahir, M. N.; Panthöfer, M.; Gao, H.; Schladt, T. D.; Gasi, T.; Ksenofontov, V.; Branscheid, R.; Weber, S.; Kolb, U.; Schreiber, L. M.; Tremel, W. *J. Mater. Chem.* **2011**, *21*, 6909.

[80] Schmid, G.; Klein, N.; Korste, L. *Polyhedron* **1988**, 605–608.

[81] Ye, Q.; Zhou, F.; Liu, W. *Chem. Soc. Rev.* **2011**, *40*, 4244–4258.

[82] Kunz, S.; Schreiber, P.; Ludwig, M.; Maturi, M. M.; Ackermann, O.; Tschurl, M.; Heiz, U. *PhysChemChemPhys* **2013**, *15*, 19253–19261.

[83] Ghosh, A.; Stellacci, F.; Kumar, R. *Catalysis Today* **2012**, *198*, 77–84.

[84] Kar, T.; Bettinger, H. F.; Scheiner, S.; Roy, A. K. *J. Phys. Chem. C* **2008**, *112*, 20070–20075.

[85] Chen, Z.; Lohr, A.; Saha-Moller, C. R.; Wurthner, F. *Chem. Soc. Rev.* **2009**, *38*, 564–584.

[86] Horswell, S. L.; Kiely, C. J.; O'Neil, I. A.; Schiffrin, D. J. *J. Am. Chem. Soc.* **1999**, *121*, 5573–5574.

[87] Akalin, E.; Akyüz, S. *Journal of Molecular Structure* **1999**, *482-483*, 175–181.

[88] de Carvalho, A. L. M. B.; Fiuza, S. M.; Tomkinson, J.; de Carvalho, L. A. E. B.; Marques, M. P. M. *Spectroscopy: An International Journal* **2012**, *27*, 403–413.

[89] Schrader, I.; Kunz, S. *in preparation.*

[90] Fenske, D.; Sonström, P.; Stöver, J.; Wang, X.; Borchert, H.; Parisi, J.; Kolny-Olesiak, J.; Bäumer, M.; Al-Shamery, K. *ChemCatChem* **2010**, *2*, 198–205.

[91] Altmann, L.; Kunz, S.; Bäumer, M. *J. Phys. Chem. C* **2014**, *118*, 8925–8932.

[92] Breiter, M. *Annals of the New York Academy of Sciences* **1963**, *101*, 709–721.

[93] Trasatti, S.; Petrii, O. *Pure And Appl. Chem.* **1991**, *63*, 711–734.

[94] Zolfaghari, A.; Chayer, M.; Jerkiewicz, G. *J. Electrochem. Soc.* **1997**, *144*, 3034–3041.

[95] Terrill, R. H.; Postlethwaite, T. A.; Chen, C.-h.; Poon, C.-D.; Terzis, A.; Chen, A.; Hutchinson, J. E.; Clark, M. R.; Wignall, G.; Londono, J. D.; Superfine, R.; Falvo, M.; Johnson Jr, C. S.; Samulski, E. T.; Murray, R. W. *J. Am. Chem. Soc.* **1995**, *117*, 12537–12548.

[96] Shin, W.; Tajima, K.; Choi, Y.; Izu, N.; Matsubara, I.; Murayama, N. *Sens. Actuators, B* **2005**, *108*, 455–460.

[97] Shin, W.; Tajima, K.; Choi, Y.; Nishibori, M.; Izu, N.; Matsubara, I.; Murayama, N. *Sens. Actuators Al* **2006**, *130-131*, 411–418.

[98] Sawaguchi, N.; Shin, W.; Izu, N.; Matsubara, I.; Murayama, N. *Sens. Actuators B* **2005**, *108*, 461–466.

[99] Yeo, Y. Y.; Vattuone, L.; King, D. A. *J. Chem. Phys.* **1997**, *106*, 392.

[100] Wu, D.-Y.; Ren, B.; Xu, X.; Liu, G.-K.; Yang, Z.-L.; Tian, Z.-Q. *J. Chem. Phys.* **2003**, *119*, 1701.

[101] Bethell, D.; Brust, M.; Schiffrin, D.; Kiely, C. *J Electroanal Chem* **1996**, *409*, 137–143.

[102] Lefrançois, A.; Couderc, E.; Faure-Vincent, J.; Sadki, S.; Pron, A.; Reiss, P. *J. Mater. Chem.* **2011**, *21*, 11524.

[103] Leibowitz, F. L.; Zheng, W.; Maye, M. M.; Zhong, C.-J. *Anal. Chem.* **1999**, *71*, 5076–5083.

[104] Zhong, C. J.; Zheng, W.; Leibowitz, F. L. *Electrochem. Comm.* **1999**, *1*, 72–77.

[105] Mensch, F. *Erdöl Kohle Erdgas Petrochemie* **1969**, *2*, 67–71.

[106] He, C.; Desai, S.; Brown, G.; Bollepalli, S. *Electrochem. Soc. Interface* **2005**, 41–44.

[107] Gasteiger, H. A.; Kocha, S. S.; Sompalli, B.; Wagner, F. T. *Applied Catalysis B: Environmental* **2005**, *56*, 9–35.

[108] Speder, J.; Altmann, L.; Bäumer, M.; Kirkensgaard, J. J. K.; Mortensen, K.; Arenz, M. *RSC Advances* **2014**, *4*, 14971.

[109] Kahsar, K. R.; Schwartz, D. K.; Medlin, J. W. *J. Am. Chem. Soc.* **2014**, *136*, 520–526.

[110] Fritz, H. P.; Geauer, H. *Z. Naturforsch.* **1978**, *33b*, 702–707.

[111] Arévalo, A.; Fernández, H.; Silber, J.; Sereno, L. *Electrochim. Acta* **1990**, *35*, 741–748.

[112] Jin, Q.; Rodriguez, J. A.; Li, C.; Darici, Y.; Tao, N. *Surf. Sci.* **1999**, *425*, 101–111.

[113] Watson, D. J.; Jesudason, R.; Beaumont, S. K.; Kyriakou, G.; Burton, J. W.; Lambert, R. M. *J. Am. Chem. Soc.* **2009**, *131*, 14584–14589.

[114] Guyon, F.; Pondaven, A.; Kerbaol, J.-M.; L'Her, M. *Inorg. Chem.* **1998**, *37*, 569–576.

# Eva Morsbach

## *Curriculum Vitae*

### Persönliche Angaben

Geburt **09.06.1987**, *Bad Honnef*

### Ausbildung

#### Akademische Ausbildung

12/2011 - laufend **Promotion**, *Katalytische Sensor-Konzepte mit funktionalisierten Nanopartikeln*, Prof. Marcus Bäumer, Universität Bremen, Institut für Angewandte und Physikalische Chemie

- Nanopartikel-Synthese und Funktionalisierung mit organischen Liganden
- Charakterisierungsschwerpunkte: TEM, IR-Spektroskopie
- Anwendung der funktionalisierten NP in katalytischen $H_2$ Sensoren

03/2014 - 04/2014
04/2013 - 05/2013 **Forschungsaufenthalt im Rahmen der Doktorarbeit**, *Universität Kopenhagen*, Prof. Matthias Arenz

- Elektrochemische Charakterisierung von Nanopartikeln

10/2006 - 10/2011 **Studium: Diplom Chemie**, *Universität Mainz*

- **Abschluss:** Diplom-Chemie, Note "sehr gut" (1,5)
- **Diplomarbeit:** Synthese von nanoskalierten thermoelektrischen Skutteruditen, Prof. Wolfgang Tremel, Institut für Anorganische Chemie
- **Diplomprüfungen:** Anorganische, Organische, Physikalische und Theoretische Chemie

09/2009 - 03/2010 **Forschungssemester**, *University of Houston*, Texas, USA, Prof. Arnold M. Guloy
High-Temperature Superconductors: Doping Effects within the LiFeAs System

#### Schulbildung

08/1997 - 03/2006 **Wiedtal Gymnasium**, *Neustadt/Wied*
Abschluss: Abitur (Note 1,6)

*Langemarckstr. 72 – 28199 Bremen*
*+49 176 62003937 • +49 421 70896247 • eva.morsbach@yahoo.com*

## Arbeitserfahrung

10/2010 - 03/2011 **Tutor zur Vorlesung:**, *Einführung in die Quantenmechanik*, Universität Mainz
Übungsstunden leiten, Korrektur der Übungsaufgaben und Klausur

04/2010 - 09/2010 **Wissenschaftliche Hilfskraft**, *Universität Mainz*, Institut für Anorganische Chemie, AK Tremel
Durchführung Nass-Chemischer Synthesen

10/2008 - 09/2009 **Tutor zur Vorlesung:**, *Allgemeine und Anorganische Chemie I*, Universität Mainz
Übungsstunden leiten, Korrektur und Erstellen der Übungsaufgaben und Klausur

09/2007 **Aushilfstätigkeit**, *Boehringer Ingelheim Pharma GmbH*, Abteilung Drug Delivery
Device- und Verpackungsentwicklung

04-2006 - 05-2006 **Praktikum**, *Lohmann GmbH und Co. KG*, Neuwied/Feldkirchen
Forschung und Entwicklung für Industrieklebstoffe

## Publikationen (als Erstauthor) und Preise

Artikel in Fachzeitschriften

E. Morsbach, J. Spéder, M. Arenz, E. Brauns, W. Lang, S. Kunz, M. Bäumer: "Stabilizing Catalytically Active Nanoparticles by Ligand Linking: Toward Three-Dimensional Networks with High Catalytic Surface Area" *Langmuir*, **2014**, *30*, 5564–5573.

E. Morsbach, E. Brauns, T. Kowalik, W. Lang, S. Kunz, M. Bäumer: "Ligand-stabilized Pt nanoparticles (NPs) as novel materials for catalytic gas sensing: influence of the ligand on important catalytic properties" *PhysChemChemPhys*, **2014**, *16*, 21243–21251

.

E. Morsbach, M. Nesselberger, J. Warneke, M. Arenz, S. Kunz, M. Bäumer: "1-Naphthylamine functionalized Pt nanoparticles: Electrochemical activity at metal surface and organic ligand", submitted

Vortrag Konferenz: 15th International Meeting on Chemical Sensors
Buenos Aires, Argentinien, März 2014

Posterpreis Konferenz: International Conference on Materials Chemistry 11
Warwick, UK, Juli 2013

## Sprachen und Sonstige Kenntnisse

Deutsch **Muttersprache**

Englisch **fließend in Wort und Schrift**

Latein **Latinum**

Software **Office-Anwendungen, Origin, EndNote, ImageJ, LaTeX**

Labortechniken **Nasschemische und Festkörpersynthesen unter Schutzgas, Transmissionselektronenmikroskopie, Infrarot-Spektroskopie**

*Langemarckstr. 72 – 28199 Bremen*
*+49 176 62003937 • +49 421 70896247 • eva.morsbach@yahoo.com*

# Reprint of own Publications

## Publication [I]

### A miniaturized catalytic gas sensor for hydrogen detection based on stabilized nanoparticles as catalytic layer

Eike Brauns, Eva Morsbach, Günter Schnurpfeil, Marcus Bäumer, Walter Lang

*Sensors and Actuators B: Chemical*, **2013**, *187*, 420–425.

---

# Publication [II]

## A fast and sensitive catalytic gas sensors for hydrogen detection based on stabilized nanoparticles as catalytic layer

Eike Brauns, Eva Morsbach, Sebastian Kunz, Marcus Bäumer, Walter Lang

*Sensors and Actuators B: Chemical*, **2014**, *193*, 895–903.

---

# Publication [III]

## Stabilizing Catalytically Active Nanoparticles by Ligand Linking: Toward Three-Dimensional Networks with High Catalytic Surface Area

Eva Morsbach, József Spéder, Matthias Arenz, Eike Brauns, Walter Lang, Sebastian Kunz, and Marcus Bäumer

*Langmuir*, **2014**, *30*, 5564–5573.

---

# Publication [IV]

## Ligand-stabilized Pt nanoparticles (NPs) as novel materials for catalytic gas sensing: influence of the ligand on important catalytic properties

Eva Morsbach, Eike Brauns, Thomas Kowalik, Walter Lang, Sebastian Kunz, and Marcus Bäumer

*PhysChemChemPhys*, **2014**, *16*, 21243–21251.

---


DOI: 10.1039/c4cp02993c

# Publication [V]

## Temperature Modulation of a Catalytic Gas Sensor

Eike Brauns, Eva Morsbach, Sebastian Kunz, Marcus Bäumer, Walter Lang

*Sensors*, **2014**, *14(11)*, 20372–20381.

---

Published with open access. The publication can be accessed at: [http://www.mdpi.com/journal/sensors]; DOI: 10.3390/s141120372

# Publication [VI]

## 1-Naphthylamine functionalized Pt nanoparticles: Electrochemical activity and redox chemistry occuring on one surface

Eva Morsbach, Markus Nesselberger, Jonas Warneke, Matthias Arenz, Sebastian Kunz, Marcus Bäumer

*submitted to New Journal of Chemistry*

---